

The Open University of Israel
Department of Mathematics and Computer Science

3DPIFCM Segmentation Algorithm for brain MRI

Thesis submitted as partial fulfillment of the requirements
towards an M.Sc. degree in Computer Science
The Open University of Israel
Computer Science Division

By

Arie Agranonik

Prepared under the supervision of
Dr. Maya Herman and Prof. Mark Last (BGU)

February 2019

Abstract.....	3
1 Introduction	4
2 Background	5
2.1 General Algorithm.....	5
2.1.1 Fuzzy c-Means (FCM) and Improved Fuzzy c-Means (IFCM)	5
2.1.2 GAIFCM	8
2.1.3 PSO.....	8
2.2 GPU computing.....	9
3 The Proposed Algorithm (3DPIFCM).....	11
3.1 Rationale	11
3.2 Originality & Contribution.....	12
3.3 Stage 1: 2D images – IFCMPSO	12
3.3.1 Algorithm Description	12
3.3.2 Assumptions.....	13
3.4 Stage 2: 3D images – 3DPIFCM	13
3.4.1 Algorithm Description	13
3.4.2 Hyper parameter values.....	16
3.4.3 Assumptions.....	17
3.5 Stage 3: Parallel 3DPIFCM.....	18
3.6 Data set Definitions.....	20
3.7 Development Toolchain.....	21
4 Runtime Analysis.....	22
4.1 IFCMPSO analysis	22
4.2 3DPIFCM analysis	22
5 Experiments	23
5.1 Evaluation parameters.....	23
5.2 3DPIFCM accuracy experiments	24
5.3 Running 3DPIFCM on synthetic data	24
5.3.1 Purpose	24
5.3.2 The experiment.....	24
5.3.3 Results.....	24
5.3.4 Analysis	25

5.4	Running 3DPIFCM on Brainweb data.....	25
5.4.1	Purpose	25
5.4.2	The experiment.....	25
5.4.3	Results.....	26
5.4.4	Analysis	26
5.5	Comparative analysis of running 3DPIFCM against FCM, IFCMPSO, GAIFCM	26
5.5.1	Purpose	26
5.5.2	The experiment.....	27
5.5.3	Results.....	27
5.5.4	Analysis	28
5.6	Evaluating new Dynamic Hyper parameters.....	29
5.6.1	Purpose	29
5.6.2	Hyper parameter H	29
5.7	3D depth– V parameter	30
5.7.1	The experiment.....	30
5.7.2	Results.....	30
5.7.3	Analysis	31
5.8	Parallel 3DPIFCM experiments.....	31
5.8.1	Introduction	31
5.8.2	Synthetic Volume experiment	32
5.8.3	Brainweb Volume Experiment	36
6	Case Study.....	38
6.1	Purpose	38
6.2	Results.....	39
6.3	Analysis	40
7	Limitations.....	40
8	Conclusions	41
9	Further Research.....	42
10	References	43

Abstract

We present a novel algorithm named 3DPIFCM, for automatic segmentation of noisy MRI Brain images. The algorithm is an extension of a well-known IFCM (Improved Fuzzy Mean Clustering) algorithm. It performs fuzzy segmentation and introduces a fitness function that is affected by proximity of the voxels and by the color intensity in 3D images. The 3DPIFCM algorithm uses PSO (Particle Swarm Optimization) in order to optimize the fitness function. In addition, the 3DPIFCM uses 3D features of near voxels to better adjust the noisy artifacts. In our experiments, we evaluate 3DPIFCM on T1 Brainweb dataset with noise levels ranging from 1% to 20% and on a synthetic dataset with ground truth both in 3D. The analysis of the segmentation results shows a significant improvement in the segmentation quality of up to 28% compared to two generic variants in noisy images and up to 60% when compared to the original FCM (Fuzzy Mean Clustering).

When executing the algorithm in a single machine we witnessed long execution times for practical clinical usage. Therefore, our second goal was to speed up the execution of 3DPIFCM by taking out parts of the algorithm and executing them as kernels on a GPU in parallel. The algorithm was implemented using the CUDA [25] framework from NVIDIA and experiments were performed on a server containing 64GB RAM, 8 cores and a TITAN X GPU with 3072 SP cores and 12GB of GPU memory. We ran the experiments for each algorithm using python with scientific computing libraries like numba and numpy that have near native performance for matrix calculations both on GPU and CPUs respectively.

We conducted experiments with the parallel version of the algorithm to itself in CPU version and also to IFCMPSO (Improved Fuzzy Mean Clustering using Particle Swarm Optimization), GAIFCM (Genetic Algorithm Fuzzy Mean Clustering) which are genetic algorithm counterparts of the 3DPIFCM algorithm. Our purpose was to test for raw execution speed in seconds of each algorithm given the same hyper parameters and same server. We also perform comparison to the original FCM algorithm in its sequential version which performs the fastest but lacks any optimization that counters for noise added to images as produced in CT or MRI scans. In our experiments we used synthetic data of varied image sizes between 32x32 pixels to 854x854 pixels. We also ran an experiment on a standard Brainweb Volume to examine the speedup in real world conditions.

Our speedup results show that the parallel version of the algorithm performs up to 27x faster than the original sequential version and 68x faster than GAIFCM algorithm. We show that the speedup of the parallel version increases as we increase the size of the image due to better utilization of cores in the GPU. Also, we show a speedup of up to 5x in our Brainweb experiment compared to other generic variants such as IFCMPSO and GAIFCM.

Those results prove that 3DPIFCM runs very well on a parallel execution environment much like the original FCM. Also, we show that this algorithm can be an adequate replacement to FCM in noisy image environments under time limited medical conditions. Since the algorithm is generic and doesn't depend on a training set there is a potential for clustering of different modalities that exist in industry such as CT, MRI and Ultrasound. All those modalities use 3D imaging and have a noisy component that can be cleared by our algorithm during segmentation. The broader potential of our work is the ability to introduce the algorithm into different clinical environments by presenting a competitive execution runtime and giving high quality segmentation results.

1 Introduction

Image segmentation in the medical domain is a very important technique in doctor assistance systems. It's used as a first step in a multistep process in medical image analysis. The result of the segmentation has an effect on all following tasks in the pipeline. Those include feature measurement, object representation, object description and even object classification. There are many methods to perform image segmentation. Those include edge detection, thresholding, region growing, clustering and supervised learning by using deep learning. Each aforementioned method has both pros and cons. No single method is considered a full solution to all modalities and image qualities [27]. In this work we focus on clustering based approach to segmentation for several reasons. First, the methods presented in this thesis are potentially applicable to different image modalities and are independent of image quality. Second, fuzzy clustering approaches are very good with medical imaging such as MRI and CT [5]. Third, we want to explore noisy medical images in 3D and see how current state of the art clustering algorithms can be improved using a 3D approach and modern optimization algorithms that can do clustering in spite of noise present in the images.

FCM [5] is one of the most popular algorithms for fuzzy clustering in the medical domain. It iterates over all pixels in the image and assigns a probabilistic score to each pixel belonging to each cluster. This way the algorithm achieves a fuzzy separation between clusters and not a hard line which is very suitable for medical images where tissues are merged. FCM performs sub optimally when there is noise in the image. This is due to its inherent nature of looking at feature attraction per pixel. Feature attraction means that each evaluation of pixels' cluster is performed by only looking at the color of all other pixels in the image and not proximate pixels. This behavior is fixed in a newer algorithm called IFCM[30][10] which balances between feature attraction and neighborhood attraction. Other works that incorporate spatial information were also introduced such as [16] but they don't optimize between feature attraction and neighborhood via an optimization algorithm. The balancing in [30] is done via optimization with a neural network. Some of this algorithms' limitations are slow convergence, suboptimal results and complex neural net implementation. GAIFCM [10] solves this problem by introducing a genetic algorithm optimization with higher accuracy. It uses GA to optimize the balance between feature attraction and neighborhood attraction.

We divide our research into two stages. The first stage is to develop a new PSO[17][23] based algorithm and compare it with GA. In stage two we develop a new 3D based algorithm that utilizes surrounding voxels of the 3D image to counteract the noisy voxels in the image. We present the IFCMPSO algorithm that performs fuzzy segmentation of medical images in 2D using the particle swarm optimization [17][9]. We analyze and test the algorithm for correctness and compare it to the GAIFCM algorithm [10]. On the basis of IFCMPSO we develop the new 3DPIFCM algorithm which performs the same function as IFCMPSO but also uses the 3D voxels of each slice thus adding more information to the optimization and improving accuracy.

First, the algorithm utilizes the voxels surrounding each segmented target voxel in order to eliminate noise in the 2D slice. Second, it introduces two hyper parameters. H is used as exponential decay parameter to control how much of each surrounding voxel has an impact on the cluster depending on the distance of this voxel from the target. V is used as a depth parameter to control how many surrounding voxels to search per target voxel in 3D space during clustering. Those two parameters are evaluated in this paper to find their optimal value.

We test all algorithms on T1 Brain MRI image from Brainweb [7]. The objective of both IFCMPSO and 3DPIFCM in our test scenario is to segment the brain images into White Matter (WM), Gray Matter (GM) and Cerebral Spinal Fluid (CSF). The IFCMPSO algorithm which works on 2D images uses a modified version of FCM for initialization of the cluster centers. The modified FCM is using a Gaussian mixture model in order to find an initial value for the cluster centers in the initialization of IFCMPSO. In our experiments we've seen that doing so avoids local minima of IFCMPSO and gives us comparable performance to GAIFCM [10].

To speed up the execution of FCM and make it parallel many works were conducted to enable the implementation of the FCM algorithm on a GPU [2][33][1][20][32][29][28]. Those works use different modifications to FCM to enable fast GPU implementations. Results and comparisons of those algorithms are detailed below. However, as of writing this paper we couldn't find any IFCM or genetic IFCM variants that run on a GPU and hence implemented 3DPIFCM. We give a brief state of related work for FCM based implementations here.

Li et al [20] implemented a parallel FCM by modifying the calculations of the membership function to run on a GPU using CUDA. They achieved a 10x speedup to the original algorithm running on a CPU. They used natural images of sizes 53k-101k on an NVIDIA GTX 260. Mahmoud et al. [1] implemented an FCM variant which uses data reduction and aggregation to cluster image data. The algorithm was tested on medical MRI and CT images of sizes 350x350 and 512x512. It was shown to be faster by 2.24 times than the best CPU variant and 23x faster than Soroosh [32] which is a traditional GPU based implementation of FCM.

In the last few years GPUs became a general purpose processing units for parallel algorithms because of new frameworks such as CUDA [25]. Since its release in 2007 by NVIDIA the GPU computation became more accessible to non-graphics algorithms and applications. Parallel algorithms using GPU have been reported to perform up to 245 times the speeds of a single CPU based algorithm [2].

Shalom et al. [29] implemented a parallel FCM algorithm on two NVIDIA GeForce 8500 cards and reached 73 fold speedup. Another experiment on 65k yeast gene expression data set of 79 dimension yielded a 140x speedup for this algorithm. Rowinska and Goclowski [28] showed a parallel FCM algorithm on polyurethane foam with fungus color images and compared to sequential FCM using C++ and MATLAB. Using C++ they reached a 10x speedup on 310k pixels and 50-100x speedup on the MATLAB version for 260k pixels.

Mishal et al [2] used a reduction technique to aggregate the membership and cluster vectors. They compared to sequential version of FCM and reached 245x speedup using shared GPU memory on a NVIDIA Tesla C2050 GPU. For the implementation of their algorithm they used C language and tested on brain images segmenting WM, GM, CSF segments.

All the works above tackled the original FCM algorithm and improved its performance using GPUs. In contrast, we look at the bottlenecks of the new 3DPFCM algorithm and design the entire algorithm on a parallel environment using the CUDA framework. The 3DPFCM is a 3D algorithm in nature. It's performing the optimization of clearing noise by utilizing the 3D environment of each voxel it's trying to segment to its respective cluster. We recognize that the majority of the work can be parallelized by sending the computation of each voxel clustering to the GPU. In such a way we utilize the massive parallel execution environment of CUDA and send small independent computations to the GPU per voxel.

Our contributions in this research are as follows, First we introduce a new clustering algorithm in 3D that can segment 2D images in 3D space and achieves 13%-60% better accuracy results in noisy images when compared to state of the art 2D variants. Second, we re-implement the original algorithm in a parallel environment namely CUDA on a GPU and achieve a speedup of up to 68x than GAIFCM. This leads to the ability of deploying our methodology in clinical settings where timely results are of the essence. Per Image the times are from 5 to 170 seconds compared to hundreds of seconds in non-optimized variants.

2 Background

2.1 General Algorithm

There are various families of algorithms to tackle the segmentation problem [27][35]. This work continues the work of [10] and therefore we chose to focus on clustering-based families following the work of [10]. Different families of algorithms were also reviewed in [10].

2.1.1 Fuzzy c-Means (FCM) and Improved Fuzzy c-Means (IFCM)

FCM is a segmentation algorithm which generalizes the c-Means algorithm, allowing soft segmentation by using fuzzy membership of each pixel to a cluster. For each pixel it assigns a membership factor to each cluster. A membership closer to 1 indicates a high degree of similarity of a pixel to other pixels in a cluster, and a value closer to 0 indicates low similarity to the data in a cluster. The FCM algorithm is an iterative clustering and produce c-partition by minimizing the weighted cost function (1) denoted as: $J_m(U, \bar{c})$. All formulas (1)-(4) are taken from [5]. Formulas (5)-

(10) are taken from [30]. All the rest of the formulas: (6a),(8a),(9a),(10a),(11),(12),(13),(14),(15) are produced in this work.

$$J_m(U, \bar{c}) = \sum_{i=1}^N \sum_{j=1}^C u_{ij}^m d^2(x_i, c_j) \quad (1)$$

Under the following conditions:

$$\begin{aligned} 0 &\leq u_{ij} \leq 1 \\ \forall i \quad \sum_{j=1}^C u_{ij} &= 1 \\ \forall j \quad 0 < \sum_{i=1}^N u_{ij} &< N \end{aligned}$$

Where:

$X \subseteq \mathbf{R}^d$ – the data set in the d -dimensional vector space (for our purposes $d = 1$)

N – the number of data points (pixels)

C – the number of clusters

$U = (u_{ij})_{1 \leq i \leq N, 1 \leq j \leq C}$ – the membership matrix (the c -partition of X)

u_{ij} – the membership factor of pixel x_i to cluster Y_j

$d^2(x, y)$ – any distance measure expressing the similarity between a sample data point and the center of a cluster.

m – the amount of fuzziness of the resulting classification ($1 \leq m < \infty$)

When $m=1$ J_m generalized to hard partition such as c -means. As m is approaching 1 the algorithm acts more like c -means. As m approaches ∞ the fuzziness factor is more dominant. In case of $m=1$ formula (2) holds.

$$u_{ij} = \begin{cases} 1, & x_i \in Y_j \\ 0, & otherwise \end{cases} \quad (2)$$

For $m > 1$, if $x_i \neq c_j$ for all i and j , (U, \bar{c}) may be locally optimal for J_m only if:

$$u_{ij} = \frac{1}{\sum_{k=1}^C \left(\frac{d(x_i, c_j)}{d(x_i, c_k)} \right)^{\frac{2}{m-1}}} \quad (3)$$

and

$$c_j = \frac{\sum_{i=1}^N u_{ij}^m \cdot x_i}{\sum_{i=1}^N u_{ij}^m} \quad (4)$$

Formulas 3 and 4 are used by iterating using simple Picard iteration, by looping back and forth from equation (3) to (4) until there are only small changes of U and \bar{c} between successive iterations[5].

The main disadvantage of the FCM algorithm is susceptibility to noise because of the distance measure $d(x_i, c_j)$ which takes into account only the pixel intensities of the target pixel vs all other pixels in the image and not the surrounding pixels' distance, i.e neighborhood attraction. The result of this limitation is degradation of the algorithms' performance with the addition of noise. As a result the segmentation reaches local minimum and cannot perform the correct noise reduction when noise levels increase above 1%.

Shan[30] proposed an improvement to FCM algorithm called IFCM which introduces neighborhood attraction and neural optimization into the FCM algorithm to overcome the problem of sensitivity to noise. The main addition of the IFCM algorithm is an improved distance measure that takes into account the distance of each pixel evaluated from the target pixel. In FCM the U membership matrix depends heavily on $d(x_i, c_j)$ as shown in formula 3 and $d(x_i, c_j)$ depends only on pixel intensities the membership is highly sensitive to noise. As a result Shan proposed a new distance measure shown in (5):

$$d^2(x_i, c_j) = \|x_i - c_j\|^2 (1 - \lambda H_{ij} - \xi F_{ij}) \quad (5)$$

There are two new parameters introduced due to the balance that need to be achieved between neighbourhood attraction and feature attraction. Those two parameters are λ, ξ that range between 0-1. In order to find the best segmentation an optimization needs to be executed to find the optimal value of those two parameters. In equation 5 there are also H_{ij} and F_{ij} which represent feature attraction function and neighbourhood attraction function respectively. H_{ij} feature attraction function calculates the feature attraction of pixels in S.

$$H_{ij} = \frac{\sum_{k=1}^S u_{kj} g_{ik}}{\sum_{k=1}^S g_{ik}} \quad (6)$$

g_{ik} is the intensity difference between the subject pixel x_i and its neighbor pixel x_k as shown in equation 7.

$$g_{ik} = |x_i - x_k| \quad (7)$$

For neighborhood attraction we use equation (8). q_{ik}^2 represents the distance between the target pixel k from the neighboring i pixel.

$$F_{ij} = \frac{\sum_{k=1}^S u_{kj}^2 q_{ik}^2}{\sum_{k=1}^S q_{ik}^2} \quad (8)$$

The relative location between pixel x_i and its neighborhood pixel x_k is:

$$q_{ik} = (X_{x_i} - X_{x_k})^2 + (Y_{x_i} - Y_{x_k})^2 \quad (9)$$

where $x_i = (X_{x_i}, Y_{x_i}), x_k = (X_{x_k}, Y_{x_k})$ and the neighborhood of x_i is

$$NB_{x_i} = \{x_k \in I : 0 < ((X_{x_i} - X_{x_k})^2 + (Y_{x_i} - Y_{x_k})^2 < 2^{L-1})\} \quad (10)$$

The algorithm is similar to FCM in the iterative manner for which it updates the membership U matrix by using the new distance function as shown in equations (6)-(10).

As a result of the introduction of the new parameters λ, ξ the algorithms needs to perform an optimization which includes calculating the cost function in equation (3) each iteration and checking if it was minimized more by choosing different values for those parameters. Shan proposed a neural network optimizer to solve this problem. Some of the disadvantages of IFCM are:

1. Bad choice of initial cluster centers might lead to poor performance.
2. In some cases the runtime is shown to be not optimal due to the complexity of the optimization model.
3. The optimizer might reach local minimum and is no guarantee for optimal values of λ, ξ [14][4][21].

To solve these problems different optimization algorithms were used that converge better and may reach global optimum. Next we review the GAIFCM algorithm which uses a genetic optimizer to find best λ, ξ .

2.1.2 GAIFCM

The GAIFCM[10] uses the GA algorithm and introduces a genome entity for which the IFCM fitness function is being calculated. Each genome can go through the crossover or mutation process. By doing so it modifies the λ and ξ parameters which might bring it closer to a global minimum error rate. The algorithm starts by initializing a population of genomes and calculating the fitness function for each. Then by the combination of crossover and mutation each genome is modified and a new population is being generated. For each new population again the fitness function is being calculated until a maximum threshold is reached or the maximum number of generations is reached. Some of the disadvantages of GAIFCM are:

1. The practical runtime of the algorithm suffers from degradation as the size of the image grows.
2. The optimization function still not guaranteed to reach global minimum as noise levels grow.
3. The algorithm uses standard FCM for the calculation of initial cluster centers to pass to GAIFCM. Since FCM can use random choice of initialization of cluster centers it can reach local minimum and give sub optimal values to GAIFCM. As a result, the search space that is being explored may not be the optimal.

2.1.3 PSO

Particle Swarm Optimization [21][15] is a nonlinear optimization algorithm introduced by Kennedy and Eberhart in 1995. We chose PSO for this work based on analysis of [13] which shows its improved accuracy and speed over GA. PSO attempts to simulate social behavior by introducing particles which move in a search space. The particles have velocity and position inside this space. Each particle is able to calculate the cost function being optimized in each iteration of the algorithm. The algorithm holds each particles' best position and the global best position. Each particle can see the neighboring particles and thus chooses to move towards the best particle in its local minima. As a result, the entire swarm moves towards the best positions in the search space. The researchers took the intuition from a swarm of fish or flocking birds after observing their behavior. For example, in the case of a flock of birds each bird can observe the birds next to it and fly in the general direction of the flock. We based our IFCMPSO and 3DPIFCM algorithms on PSO optimization. The algorithm is described below as Algorithm 1.

Algorithm 1: Generic PSO algorithm

Input: S – number of particles, d – number of dimensions, f() – optimization function, $\epsilon > 0$ – stop criteria
Output: Best particle that minimizes the f() function

1. For each particle $i = 1 \dots S$ do
2. $x_i = U(b_l, b_u)$ – initialize particle's positions uniformly
3. $p_i = x_i$ – initialize best particle's know position
4. If $f(p_i) < f(g)$ then
5. $g = p_i$ – update swarms best position
6. $v_i = U(-|b_l, b_u|, |b_l, b_u|)$ – initialize particle's velocity
7. While $ch > \epsilon$ – check if minimal change in position smaller then threshold
8. For each particle $i = 1 \dots S$ do
9. For each dimension $d = 1 \dots n$ do
10. $r_p, r_g = U(0,1)$ – random numbers between 0,1 in a Uniform distribution
11. $v_{i,d} = \omega v_{i,d} + \varphi_p r_p (p_{i,d} - x_{i,d}) + \varphi_g r_g (g_{i,d} - x_{i,d})$ – update particle velocity
12. If $f(x_i) < f(p_i)$ then
13. $p_i = x_i$ – update particle's best position
14. If $f(p_i) < f(g_i)$ then
15. $g = p_i$ – update swarms best position
16. $ch = \text{smallest change in } f$
17. Return g

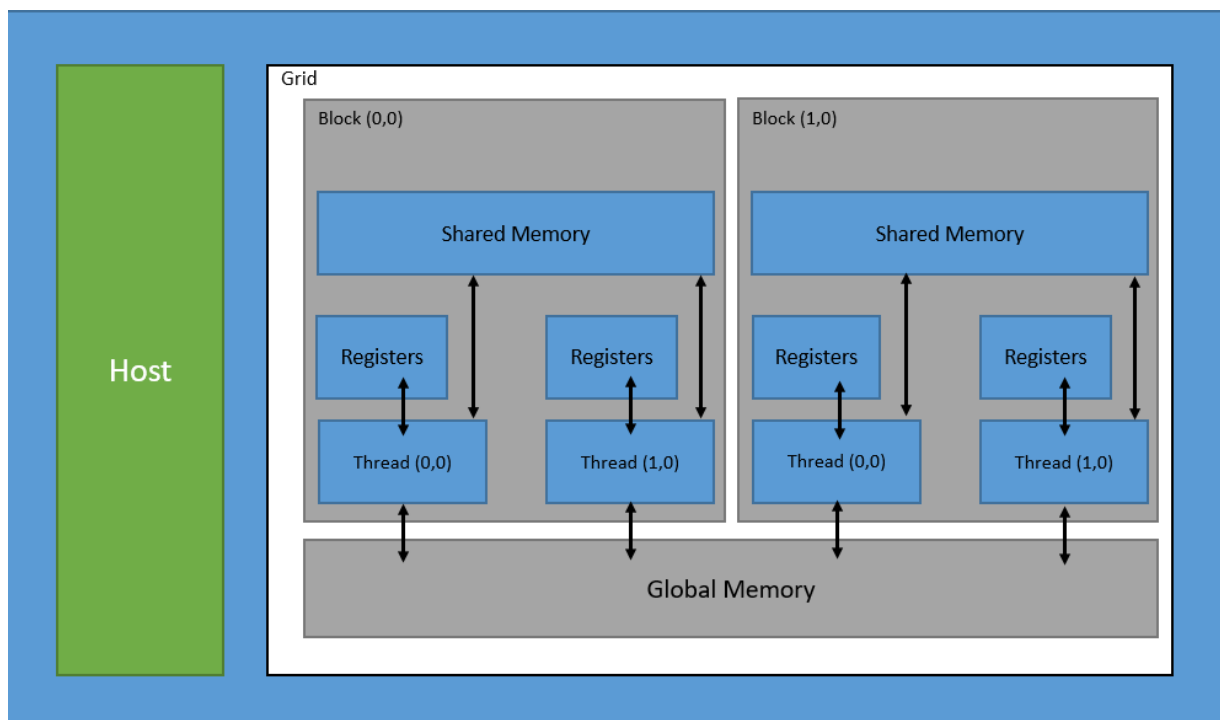
PSO has some advantages to GA in optimization problems in the search space [13]. First, the authors in [13] evaluated PSO vs GA on 8 different sets of problems while measuring quality and computation cost. They reached the conclusion using t-tests that PSO uses less function evaluations than GA [13] while reaching similar quality and thus more efficient. Second, due to the fact that PSO holds two populations for each particle (pbest and current position), this allows for more diversity and exploration than GA.

2.2 GPU computing

The standard NVIDIA GPU is built by having many processing units called scalar processors (SPs). Each SP is assigned to a block of processors which have shared block memory. This memory is very fast and is accessible to each thread running within a block. In addition, the GPU has a device memory called global memory. The modern GPU's have device memory that ranges in Gigabytes. Normally, a general purpose algorithm running on a GPU will execute thousands of threads. Each thread will have access to local (register based), shared and global memory. Each algorithm designed for the GPU must have thread contention and locks to prevent other threads modifying memory locations that are not desired.

As can be seen in Figure 1 the host on the left is the CPU and main memory. At the first stage of each parallel algorithm data is moved from host to global memory to be processed by kernels. Kernel is a small execution function used by the GPU by many threads running concurrently. Each thread that picks up data from global memory executes the kernel on this data running inside a block. The blocks are located inside the grid. Each thread may use register memory for local variables. This memory is very fast but limited in size. Shared memory is used by multiple threads running inside a block thereby utilizing sharing between local block threads for some memory operations. Figure 2 shows that general GPU structure.

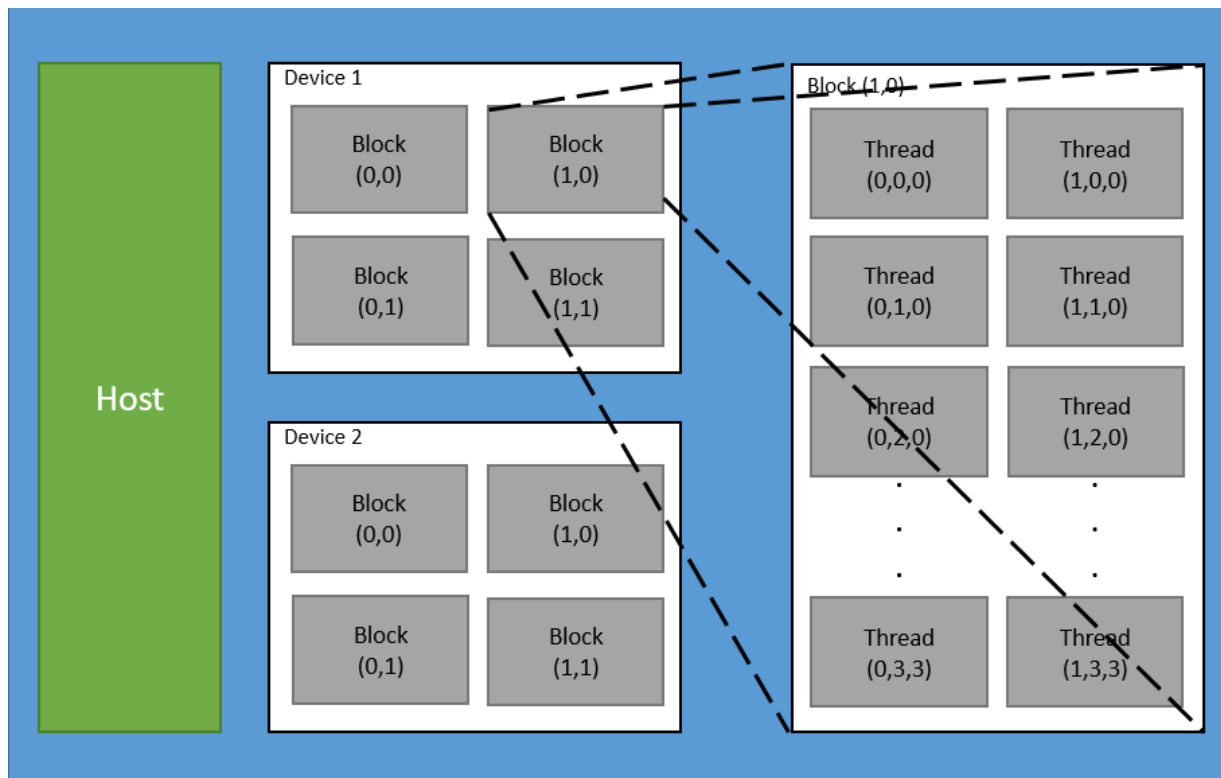
Figure 1: GPU structure.



The CUDA API enables to use a new programmatic model on a GPU. This API hides hardware details from the programmer and enables compiler directives which are annotations in the code. Those directives will execute in parallel when compiled with the nvcc compiler and run directly on the GPU device. As a result, many applications and algorithms that were previously targeted to CPU's are now running in a parallel framework on a GPU [11]. Those include scientific, analytic and engineering applications [33][31].

As can be seen in figure 2 the host sends the kernel code to the GPU to be distributed in many blocks and threads on a single grid. Once the code is run each kernel will handle a different part of the data stream. The kernel will receive block id, thread id and block dimension as part of its input. As a result, it is possible to control which part of the global data the thread is going to handle by multiplying block id by block dimension and adding thread id to find a location in a global array. Because of this parallel structure it's possible to send large amounts of data to the global memory once and have the kernels process it in parallel. Figure 2 shows the CUDA processing model.

Figure 2: CUDA processing model.



CUDA development model consists of combination CPU and GPU code. The CPU code is normally used for complex data structures and control flow while the GPU code is targeted for massively parallel operations such as SIMD operations (Single Instruction Multiple Data). The algorithms that are developed for GPU utilization consist of kernels that are designed to run on the GPU and control code which executes on CPU. The algorithms typically transfer large amounts of data to GPU and then run the CPU control code. The control code will execute kernels as appropriate and finally results will be moved back from GPU to CPU for display.

3 The Proposed Algorithm (3DPICFM)

3.1 Rationale

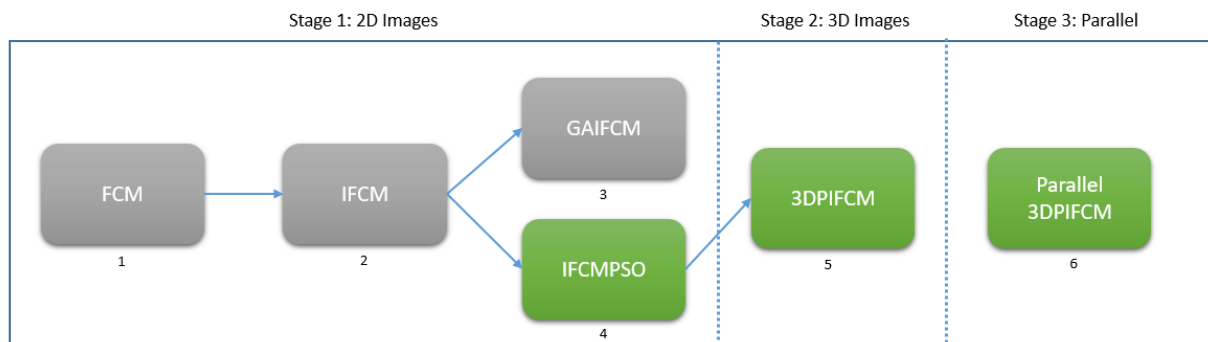
The development of 3DPICFM has been done in three stages. In stage one a 2D algorithm was developed which is equivalent to GAIFCM but uses PSO instead of GA. The reason for choosing PSO was for higher speed of convergence [13] and simpler implementation. Also, in the development of IFCMPSO, better initialization of the cluster centers was made to avoid local minima. This was done using a Gaussian Mixture Model by giving C – number of clusters as input. We discuss IFCMPSO and the new initialization of cluster centers in section 3.3.1

In stage two a new 3D version of IFCMPSO was developed we call 3DPICFM. The rationale of moving from 2D to 3D for noise correction was that since medical imaging includes mainly organs that have methodically arranged voxels (volume pixels) of same tissue type in 3D space we could utilize those voxels to correct noise during segmentation.

In stage three we developed a parallel version of the 3DPICFM algorithm on a GPU to test its speed vs the older version and previous versions of other IFCM variants that run in sequential manner.

This new algorithm runs iteratively on each voxel in the 2D image much like IFCM. The main difference is that at each iteration of the algorithm when trying to classify a voxel into a cluster it looks at voxels surrounding the target voxel in 3D. When examining each voxel separately in the 3D image we can extract the IFCM features in order to achieve better noise reduction in 2D. In addition, by adding the 3D X order features to the algorithm’s attraction function we give higher weight to closer voxels and lower weight to distant voxels. We add the 3D features to the attraction equations (6, 8, 9). In figure 3 we show the evolution of the algorithms reviewed and the new algorithms we developed.

Figure 3: Evolution of fuzzy clustering algorithms described in this thesis. Green boxes are new algorithms presented in this work.



Notation:

1. Fuzzy c-means algorithm. There is no noise reduction. It’s using only feature attraction (pixel colors) to determine clusters. It’s a very popular algorithm that works well with clean images.
2. Improved fuzzy c-means. Used to counter noisy pixels in 2D images. It’s using a neural network optimization of neighborhood attraction and feature attraction. Also, there is a new cost function which looks at proximity and color of pixels.
3. Genetic algorithm IFCM. It’s using same cost function as 2 but improving optimization algorithm by using GA.
4. PSO based IFCM. It’s using same cost function as 2 with PSO optimization and change in initialization of cluster centers in modified FCM.
5. 3D version of PSO based IFCM with additional hyper parameters for depth and exponential decay. It’s utilizing the 3D nature of the medical image to counter noisy voxels.

6. Parallel version of 3DPIFCM on a GPU using CUDA. This implementation improves running speed.

3.2 Originality & Contribution

Our original contributions in developing 3DPIFCM come in three folds:

1. The development of the 2D version named IFCMPSO compares well to GAIFCM but converges faster due to PSO optimization.
2. The 3DPIFCM algorithm is compared to state of the art GAIFCM, IFCMPSO and also FCM for segmentation accuracy at different levels of noise ranging from 1% to 20%. We can observe that 3DPIFCM outperforms the state-of-the-art by up to 60% at lower level noise down to 13 % at higher levels.
3. We implement a parallel version of 3DPIFCM and show that it is 68x faster than the slowest IFCM variant. This leads the way to deployment of the algorithm in clinical settings.

3.3 Stage 1: 2D images – IFCMPSO

3.3.1 Algorithm Description

We first describe our modification to the original FCM in algorithm 2:

Algorithm 2: Modified FCM Algorithm

<u>Input:</u> m – amount of fuzziness, c – number of clusters, ϵ – stopping threshold, X - image
<u>Output:</u> U membership matrix. Each pixel is given a probability to be in each cluster.

1. Fix $m > 1, c \geq 2$ and the stopping criteria $\epsilon > 0$
2. Initialize $U^{(0)} = [u_{ij}]$ matrix of size $N \times C$.
3. **Initialize vector of centers using GMM $C^{(k)} = gmm(c)$**
4. Calculate the vector of centers $C^{(k)} = [c_j]$ using $U^{(k)}$ and equation (4).
5. Update $U^{(k)}$ to $U^{(k+1)}$ using equation (3).
6. If $\|U^{(k+1)} - U^{(k)}\|_{\infty} < \epsilon$ stop, else repeat steps (4-6).

Modified FCM Description:

Lines 1-2: initialize the U cluster matrix.

Line 3: The main change compared to the original FCM is instead of initializing vector of cluster centres randomly we run a Gaussian Mixture Model on the image using same number of clusters C . This gives us good estimates and avoids possible local minima that FCM might reach in noisy images. This change was done because FCM often reaches local minima in cluster centres and returns a suboptimal result to the following IFCMPSO algorithm. By doing this change we avoid such phenomena in noisy MRI images.

Lines 4-6: calculate vector centers and update U matrix. Check if stop criteria is reached.

IFCMPSO is described in algorithm 3.

Algorithm 3: IFCMPSO Algorithm

Input: img - a 2D matrix of pixel intensities, c – number of clusters, m - fuzziness, ϵ – stop criteria , L – depth level
Output: centers, U – membershipMatrix

1. cluster_centers1, U1 = Modified_FCM (img, c, ϵ , m)
2. λ , ξ . cluster_centers2, U2 = PSO (ifcm_step(), cluster_centers1, U1, img, L, m, c)
3. cluster_centers3, U3= IFCM (img , λ , ξ . cluster_centers2, U2, L, m, c, ϵ)

return cluster_centers3, U3

IFCMPSO Algorithm description:

1. A modified version of FCM which uses a Gaussian mixture model [12] for initialization of cluster centers is used instead of a random choice. As a result, local minima is avoided in contrast to optimizations that were produced in earlier experiments.
2. Cluster centers and membership matrix U are used to feed to PSO as initial parameters. In addition, the IFCM_STEP function which performs the optimization according to formulas (1, 3, 4, 5-10) is used. In our description in algorithm 3 λ , ξ are the particles returned from PSO that are optimal to the cost function **ifcm_step()** and image **img**. Sensitivity analysis of λ , ξ was done in [30,10].
3. Once we obtained the optimal parameters λ , ξ for the image a full execution of IFCM algorithm is performed. This finally returns a new membership matrix and cluster centers that are returned by the algorithm.

3.3.2 Assumptions

1. For M parameter a value of 2 is used. Previous studies show that the optimal value is 1.5 to 2 [10].
2. The value of L=2 is used based on [10] and [30].
3. PSO max iterations is 150. This number was chosen after examining runtime and convergence as a balance between speed and quality.
4. Swarm size of 50 was used. Similar to [10] similar hyper parameter for breath of search was used as in GA. Again, we struck a balance between speed and quality as in [10].

3.4 Stage 2: 3D images – 3DPIFCM

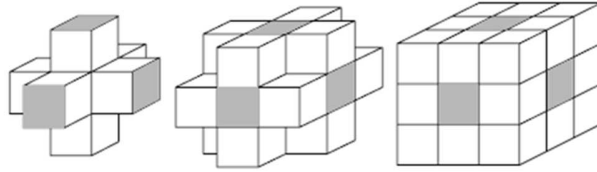
3.4.1 Algorithm Description

The 3DPIFCM algorithm uses N^{th} order features for segmentation. Those features represent the voxels around the target voxel that is being segmented. The image segmented is still in 2D but voxels in 3D space help to clear the noise. The algorithm iterates over all voxels in the 2D image and in an inner loop examines all voxels in the neighborhood of that center voxel in 3D. It uses feature attraction and neighborhood attraction like IFCM but instead of using a neural network for optimization of λ and ξ it uses PSO. At the start of the algorithm it runs a modified version of FCM that initializes the cluster centers to be in a good position to avoid local minima. In addition, it uses two new parameters h, v as input that control the exponential decay of each neighborhood voxel and the depth of search respectively. First we define the area around the target voxel as shown in (10) to modified 3D version (10a).

$$NB_{ik} = \left\{ x_k \in I : 0 < \left((X_{x_i} - X_{x_k})^2 + (Y_{x_i} - Y_{x_k})^2 + (Z_{x_i} - Z_{x_k})^2 < 2^{L-1} \right) \right\} \quad (10a)$$

Figure 4 shows a definition of the features in (10a) for L=1, 2, 3 from left to right.

Figure 4: First, second and third order voxels respectively from left to right. First order has 6 neighbouring voxels to centre voxel, second has 18 and third has 26. All voxels surrounding the central voxel on the left image are first order. The ones surrounding the central voxel on the central image are second order and voxels surrounding second order are third order. In section 5.7.2 we examine the contribution of the number of neighbours to the segmentation quality in different noise levels for Gaussian noise.



We modify equation (9) to (9a) as follows:

$$q_{ik} = (X_{x_i} - X_{x_k})^2 + (Y_{x_i} - Y_{x_k})^2 + (Z_{x_i} - Z_{x_k})^2 \quad (9a)$$

Equation (9a) looks at each voxel in (10a) and does a squared sum on all axis. This represents the squared difference between the color of target voxel and a surrounding neighborhood voxels. We also assign a higher weight to N order voxels and a lower weight to N+1 order voxels. This is done according to w vector which is shown in (6a) and (8a) that are modified versions of (6) and (8) respectively. We introduce a new vector w such that the elements of w sum to 1. This vector represents the weighted decaying importance of proximity of each voxel according to the originating group.

The size of w vector is v such that $\sum_{r=1}^v W_r = 1$. If we assign each element in the vector to be $1/v$ equations (6a) and (8a) will behave exactly like equations (6), (8). The neighboring voxels in (10a) are divided into v sub groups. The v parameter will determine the depth of search for each target voxel. If $v > 3$ the next set of voxels will be at least 2 voxels away from the target voxel. This may extend the reach of the clustering but may diminish the proximity ingredient. For parameter v a value of 2-5 was experimented with. In part (g) of the results section V we experiment with different values of v. The sub groups are mutually exclusive and $\sum_{r=1}^v NB_r \in NB_{x_i}$. The sub groups complement the entire set of neighboring voxels in (10a).

$$H_{ij} = \sum_{r=1}^v W_r \frac{\sum_{k=1}^{S_r} u_{kj} g_{ik}}{\sum_{k=1}^{S_r} g_{ik}} \quad (6a)$$

$$F_{ij} = \sum_{r=1}^v W_r \frac{\sum_{k=1}^{S_r} u_{kj}^2 q_{ik}^2}{\sum_{k=1}^{S_r} q_{ik}^2} \quad (8a)$$

We define a decay constant h . In order to populate the w vector we use an exponential decay equation (11). More information about the h and v constants and their optimal values can be found in section 5.6.

$$W_i = \frac{e^{-\frac{i}{h}}}{\sum_{r=1}^v e^{-\frac{r}{h}}} \text{ where } i = 1..v \quad (11)$$

Equation (11) is based on half-life exponential decay [34][19]. The formula is meant to lower the importance of each order of voxels as further they are located from the center. For example, if size of vector is $v=3$ and $h=1.1$ then the w vector will look like $w = [0.63, 0.25, 0.12]$ thus assigning a higher importance to first order voxels, lower importance to second order and much lower to third. The h parameter is an exponential decay parameter that determines the ingredient of each voxels' contribution to the final distance function according to the group membership.

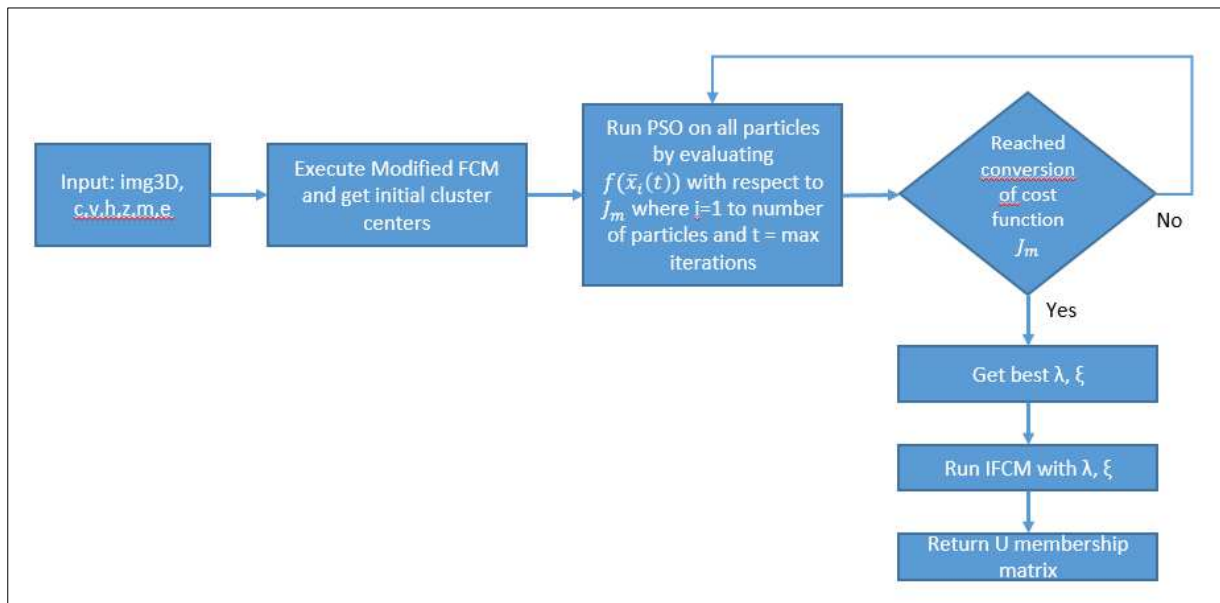
The higher the h parameter the more weight will be assigned to the furthest voxels and less to the closest. If the h parameter is around 0.5 than 86% of the weight will be to first level voxels closes to the target voxel. On the other hand if the h parameter is very high (for example 100) then w vector will look like $w = [0.33, 0.33, 0.33]$ thus assigning equal importance to each order of voxels from first to n^{th} order. We closely discuss both v and h parameters in section V and experiment with different values to achieve highest performance.

We define the cost function in (12) as the standard FCM cost function J_m with the addition of v and h as parameters. The modified distance function is defined in (6a, 8a, 9a).

$$J_m(U, \bar{c}, h, v, m, \epsilon) = \sum_{i=1}^N \sum_{j=1}^c u_{ij}^m d^2(x_i, c_j, h, v, m, \epsilon) \quad (12)$$

This cost function already accepts both new parameters h and v and all other standard IFCM parameters m and ϵ . Below we show the flowchart of 3DPIFCM and a more detailed pseudo code for the algorithm. Both are shown in Algorithm 4 flowchart and Algorithm 4 description respectively.

Algorithm 4: 3DPIFCM algorithm flowchart



Algorithm 4: 3DPIFCM Algorithm

Input: img3d - a 3D matrix of pixel intensities, c – number of clusters, v – depth parameter, h – exponential decay, z – which slice in z axis to segment, m – fuzziness, ϵ – stop criteria
Output: centers, U – membershipMatrix

1. img = img3d[z]
 2. cluster_centers1, U1 = Modified_FCM (img, c, ϵ , m)
 3. Generate a random swarm of P particles in 2 dimensional space (we use D=2 since there are two optimization parameters).
 4. Evaluate fitness of each particle in the swarm $f(\bar{x}_i(t))$ with respect to the cost function J_m .
 5. If $f(\bar{x}_i(t)) < pbest_i$ then $pbest_i = f(\bar{x}_i(t))$ and $\bar{x}_{pbest_i} = \bar{x}_i(t)$ where $pbest_i$ is the current best fitness achieved by the i-th particle and \bar{x}_{pbest_i} is the corresponding coordinate.
 6. If $f(\bar{x}_i(t)) < lbest_i$ then $lbest_i = f(\bar{x}_i(t))$, where $lbest_i$ is the best fitness over the topological neighbors.
 7. Change the velocity v_i of each particle: $\bar{v}_i(t) = \bar{v}_i(t-1) + p_1(\bar{x}_{pbest_i} - \bar{x}_i(t)) + p_2(\bar{x}_{lbest_i} - \bar{x}_i(t))$ p_1 and p_2 are random constants between 0 and 1. Fly each particle to its new position $\bar{x}_i(t) + \bar{v}_i(t)$
 8. Go to step 4 until convergence (i.e small changes to J cost function).
 9. cluster_centers2, U2, λ , ξ = \bar{x}_{pbest_i} variables.
 10. cluster_centers, U = IFCM (img, λ , ξ , cluster_centers2, U2, v, m, c, ϵ)
 - 11.
 12. Return cluster_centers, U
-

Algorithm 3DPIFCM Description:

1. Assign the z slice to a new variable
2. Run the modified FCM with Gaussian mixture model instead of random initialization of centers.
3. Generate random particles to evaluate parameters λ , ξ .
4. Steps 4-9 are running the PSO algorithm and executing the step function of 3DPIFCM at each step. The step function includes evaluating equation 1 with modified formulas 6a, 8a, 9a.
10. Take the best particle in the swarm after the swarm finished executing and get values λ , ξ , cluster centers and membership matrix.
11. Execute standard IFCM with correct λ , ξ , parameters and correct membership matrix and cluster centers.
12. Return the U membership matrix and cluster centers.

3.4.2 Hyper parameter values

We make certain assumptions in all implementations of variants of FCM. The hyper parameters we use for 3DPIFCM are shown in table 1. The choice of hyper parameters builds upon the works of [5][9][10][30]. For the new hyper

parameters we introduce in this work (shown in table 2) we explore their effect on performance in sections 5.6 and 5.7.

Table 1: Hyper Parameters Values

Hyper Parameter	Value	Description	Algorithms	References
M	2	Fuzziness	All	[5]
E	0.01	Stop criteria	All	[10]
L	2	2D Neighbourhood level	GAIFCM, FCM, IFCMPSO	[30]
Max iterations	150	Another stop criteria in case we don't reach epsilon	All	[10]
PSO swarm size	50	Number of particles in the swarm	3DPIFCM, IFCMPSO	
omega	0.5	Velocity scaling factor	3DPIFCM, IFCMPSO	
phip	0.5	Scaling factor to search away from the particle's best known position	3DPIFCM, IFCMPSO	
phig	0.5	Scaling factor to search away from the swarm's best known position	3DPIFCM, IFCMPSO	
Pso_max_iter	20	The maximum number of iterations for the swarm to search	3DPIFCM, IFCMPSO	
minstep	1e-8	The minimum step size of swarm's best position before the search	3DPIFCM, IFCMPSO	
minfunc	1e-8	The minimum change of swarm's best objective value before the search	3DPIFCM, IFCMPSO	

In addition to the static hyper parameters we research the dynamic hyper parameters that are new to 3DPIFCM. We show their ranges in table 2.

Table 2: Dynamic Hyper Parameters Ranges for 3DPIFCM

Hyper Parameter	Name	Value range	Description
h	Exponential decay	0.01 - 100	Determines the ingredient of each voxels' contribution to the final distance function according to the group membership.
v	Depth	2 - 5	Determines the depth of search for each target voxel.

3.4.3 Assumptions

The main premise of our new algorithm is that image comes in 3D format. This is most common in medical imaging domain such as MRI and CT scan where there are 3 planes of view. Another assumption is that the images come in grayscale colors. This is also most common format in medical imaging. Although our algorithm should be able to handle RGB colors, this option was not tested during this work.

Some assumptions on hyper parameters are:

1. Same assumptions as in section 3.3.2 hold here for 3DPIFCM.

2. The new parameter h values of 0.01 to 100 were chosen. Those values represent experiments that were performed in experiments section 5.6.
3. In the new depth parameter values of 2-5 were chosen. Those values represent experiments that were performed in experiments section 5.7.

In addition, the algorithm was test image sizes ranging from 32x32 to 854x854. Standard medical image sizes come in 512x512 pixels in MRI which are well within those bounds. Although there is no theoretical or computational limit to the size of the images we assume standard medical sizes.

3.5 Stage 3: Parallel 3DPIFCM

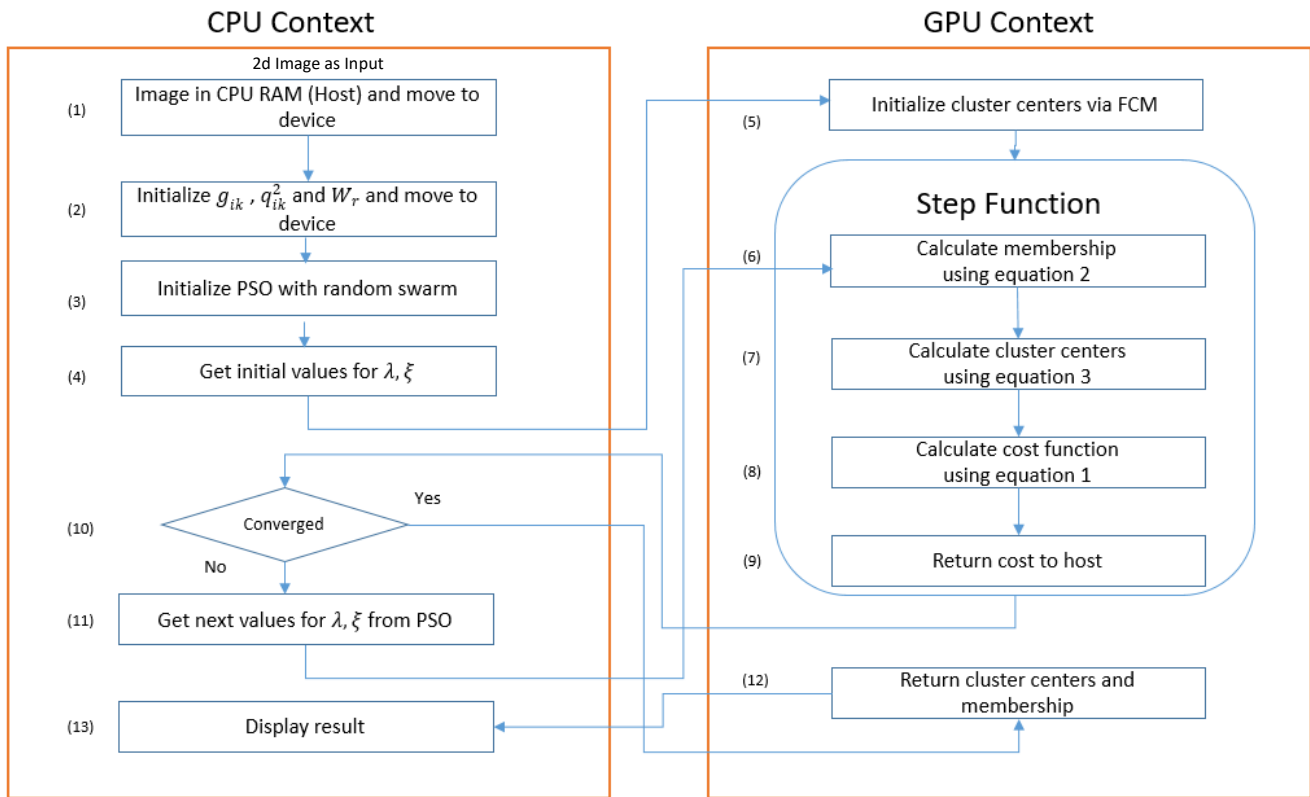
In 3DPIFCM the goal was to parallelize bottleneck operations that take most time on CPU. The parallel operations are done at a voxel level on the GPU. Since the algorithm accepts an image as input and runs on every pixel on this image sequentially, the most costly operation is therefore the per pixel operation which we called the IFCM step function. Also, as can be examined in the original step function it's independent from other operations that were done in previous steps. As a result, it's a perfect candidate for penalization to be executed on the GPU as a kernel function.

The step function runs a single iteration of segmentation with preset λ, ξ parameters as part of the iterative optimization algorithm. This function $f(\bar{x}_i(t))$ as shown in algorithm 1 is running through each voxel in the slice of a particular z axis image and recalculating the membership matrix and cluster centers including the cost function as shown in equation (1).

For each iteration of the step function equations 2,3,4,5,6a,7,8a,9a,10a need to be executed in order to calculate equation (1) and get the new cost which will be evaluated against previous iterations of $J_m(U, \bar{c})$ until reaching convergence. Our implementation of 3DPIFCM on the GPU is utilizing heavy caching of pre calculated feature maps and neighborhood maps that are calculated once at the initial steps of the algorithm and passed to the GPU as matrices. This reduces considerable GPU time for each calculation of voxel per iteration. Next we examine the algorithm and caching of parameters.

First we look at the new equations we introduced 6a, 8a, 9a, 10a for possible caching optimization. In equations 6a, 8a we can see that g_{ik}, q_{ik}^2 and W_r are matrices that are not modified between each step function $f(\bar{x}_i(t))$. Therefore it is possible to pre calculate them in the initial step on the CPU, transfer to the GPU and cache them for further iterations. Since the main membership and cluster centers equations (2), (3) are modified in each iteration of the step function they cannot be cached on the GPU. As a result they are also calculated on the GPU memory for efficient optimization and runtime. We show a flowchart of the 3DPIFCM algorithm on the GPU in Algorithm 2.

Algorithm 5: 3DPIFCM on GPU



Algorithm 3DPIFCM on GPU description:

Input:

- img3d – A 3D matrix of pixel intensities
- c – Number of clusters
- v – Depth parameter
- h – Exponential decay
- z – Slice in z axis to segment
- m – Fuzziness
- ϵ – Stop criteria

Output:

- Centers – the centroids of each cluster.
- U – Membership Matrix

Flowchart:

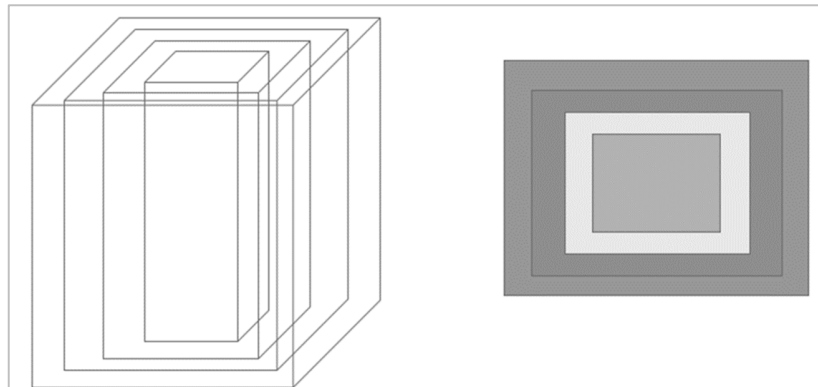
1. Prepare the image, normalize it and move to device memory (GPU).
A normalize via min max so that each voxel value is between 0 and 1 across the entire 3D image. Consequentially, the results are more stable during the optimization of PSO and the cost function.
2. Initialize the parameters g_{ik} , q_{ik}^2 and W_r from equations 6a, 7, 8a, 9a, 10a and move the matrices to device memory. The cost of initialization of the parameters on the CPU is negligible to the entire runtime of the algorithm.

3. Initialize PSO swarm. According to the PSO algorithm as depicted in Algorithm 1 it's using velocity and position of the particle to optimize the cost function. This initialization ultimately creates random combinations of particles with different λ , ξ values ranging from 0 to 1.
4. Get initial values for λ , ξ from initial position and velocity of PSO swarm.
5. Execute FCM on device and get initial cluster centers and membership matrix (C, U respectively). As FCM runtime is negligible in comparison to rest of the algorithm we used an approach similar to [32] for FCM on GPU approach.
6. Calculate membership matrix on the GPU using equation 2. This calculation is running in parallel using thread per voxel approach as in [2].
7. Calculate cluster centers on GPU for values λ , ξ using equation 3 (which utilizes new equations 6a-10a). Here too we run thread per voxel as in [2].
8. Calculate Cost function using equation (1) on GPU.
9. Return the result of cost function to CPU for loop control.
10. Check if convergence of ϵ (algorithm 4) was reached in this iteration. If yes go to 12, otherwise go to 11.
11. Retrieve λ , ξ from PSO according to swarm velocity and position and go to step 6.
12. Get final clustering centers and membership result and move to host.
13. Display membership result on host.

3.6 Data set Definitions

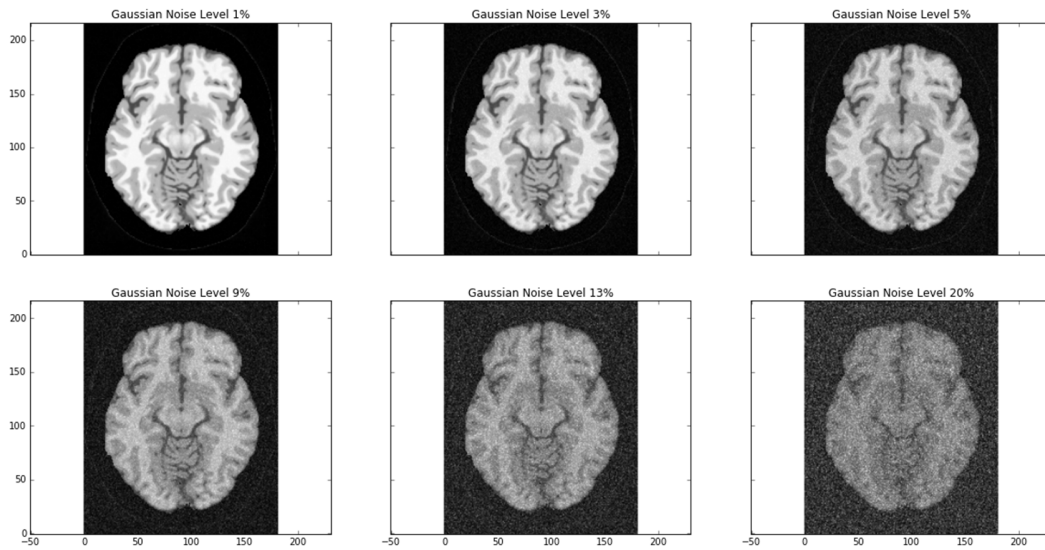
Two different datasets were used to test the accuracy of the segmentation. The first dataset is a synthetic dataset that includes 4 squares of different colors in grayscale one inside the other. The volume is the same size in pixels as Brainweb^[7] which is 181x217x181 voxels. This is the standard size of the Brainweb[7] volume that is published for research and we copied it for comparison. Gaussian granular noise was added to the synthetic data ranging from 16% to 27%. The high noise ratio is because the data is homogeneous and all algorithms perform very well under lower noise levels for this set. The synthetic data is shown in figure 5.

Figure 5: on the left is a 3D representation of the synthetic data of size 181x217x181 voxels. Each cube will have a difference color. On the right is a top view of the cube.



The second data set is Brainweb[7] T1 simulation of an adult brain. several volumes of varying amounts of noise were created ranging from 1% to 20%. Both Gaussian and Poisson noise in same levels were tested since Gaussian is more prevalent for MRI scans and Poisson for CT scans. All noise levels were homogeneous in our tests. In addition, we examined the variability of noise and statistical significance of the algorithm's performance. Figure 6 shows a sample of Brainweb[7] data.

Figure 6: Brainweb[7] data with Gaussian noise level from 1% to 20%.



As can be seen in the Brainweb[7] data in higher noise levels the image becomes unclear and tissues are indistinguishable.

3.7 Development Toolchain

The implementation of the algorithms in all cases was done in python 2.7 with numpy for numeric computations to speedup performance. In addition, we used the numba[26] package to JIT compile the functions that make up the most costly operations such as the step functions in FCM, IFCM, 3DPIFCM and GAIFCM. The step functions go through the entire image pixel by pixel and perform the calculations of the clusters and depicted in formulas 1-11 inclusive. The compilation of Python functions is done via a specially annotated Python which is typed and similar to c in syntax. This is done via the numba framework.

The JIT compilation step makes the implementation nearly identical to a native C/C++ variant. We wanted to make the algorithms run as fast as possible but still use a high level scientific language. Although in this paper we are not analyzing the speed of the implementations in terms of raw second performance it was still necessary to write optimized code to increase number of experiments and test for hyper parameters. The research stack also included using nibabel[8] for reading medical image file types such as Nifti and matlab matrices in MINC[22] format. In order to visualize the results the Jupyter Notebook stack was used.

The parallel algorithm is also implemented entirely with open source tools. We used JIT compiled extension Numba[18] with CUDA support. The Numba package allows us to compile functions to C code both for CPU and GPU usage. The nvcc annotations that are used within Numba are similar to the original C language compiler annotations that are present in C/C++ code. For example, when JIT compiling a function to CPU usage we use an annotation such as `@jit(nopython=True)` and require limited python language to enable to execute it. In order to enable GPU execution we use `@cuda.jit` annotation before the function.

When using such an annotation before a function we ensure that this function becomes a GPU kernel function. In order to pass parameters to this function we first must transfer them to the GPU as a preprocessing step. Once this function is activated CUDA enables us to use parallelism of block and threads. In our implementation we assign a thread for each voxel that is being calculated against each cluster.

4 Runtime Analysis

We analyze the asymptotic performance of 3DPFCM algorithm together with IFCMPSO. Analysis of GAIFCM, IFCM, FCM exist in [10]. We compare this data to the new algorithm. First we examine the performance of FCM as stated in [10][5]. FCM runs an iterative process which has max number of iterations that are defined by a parameter. For each iteration there is an evaluation of the entire image. We assume image size N pixels and cluster size C . Each membership calculation of FCM takes $\theta(C^2 \cdot N)$. As shown in [10][5] the overall asymptotic performance of FCM is therefore $O(\maxIterations \cdot C^2 \cdot N)$.

IFCM modifies the distance function to account for noise. A new parameter S is added as a neighbourhood parameter that accounts for distance measure from target pixel being evaluated in each iteration to all pixels in S . the overall performance of IFCM is shown to be $\max\{O(\maxIterations \cdot S \cdot C \cdot N), O(\maxIterations \cdot C^2 \cdot N)\}$. Since IFCM uses FCM as an initial segmentation to get initial cluster centres we take the maximum of either the running time of FCM or the evaluation of IFCM with the S parameter.

GAIFCM as described in [10] uses a population and generation parameters. It runs an iterative process by which all the population is affected and each genome is running a full step function of IFCM which evaluates to $O(S \cdot C^2 \cdot N)$. If we assume S a small constant, eventually Frizon et al shows that the effective asymptotic performance of the algorithm is $\Theta(generationsCount \cdot populationSize \cdot C^2 \cdot N)$

In order to evaluate 3DPFCM we first evaluate IFCMPSO since both algorithms work with the PSO optimization function.

4.1 IFCMPSO analysis

Particle Swarm Optimization works by first selecting the size of the swarm which we denote SW . The swarm consists of particles that have a position and velocity in the search space of the swarm. Each particle has a dimension which consists of the number of parameters the algorithm is trying to optimize.

First the algorithm runs FCM which is $\theta(C^2 \cdot N)$

The main loop is iterating each particle in the swarm for each dimension. For each iteration the objective function is evaluated which has a cost of $\Theta(C^2 \cdot N)$.

During the test of the objective function there is an update to both velocity and position of the swarm according to $v_{i,d} = \omega v_{i,d} + \varphi_p r_p (p_{i,d} - x_{i,d}) + \varphi_g r_g (g_{i,d} - x_{i,d})$. The position is updated by evaluating the objective function and getting the result of segmentation.

This process runs max number of iterations until minimal change detected or max iterations is reached.

The 4 steps shown above and fully in algorithm 3 define the asymptotic performance to be $\Theta(SW \cdot d \cdot \maxIterations \cdot C^2 \cdot N)$. As in our case the d parameter is not significant (1 or 2) the formula is reduced to $\Theta(SW \cdot \maxIterations \cdot C^2 \cdot N)$

Asymptotically this implies that GA and PSO have similar performance. Nevertheless, research shows in [13] that PSO outperforms GA by at least factor of 2 due to faster convergence.

4.2 3DPFCM analysis

Our new 3DPFCM algorithm also uses PSO as an optimizer but adds a new dimension to the proximity and feature equations. This measure is the S parameter which indicates how many voxels to examine in each iteration of the modified IFCM step function. Since we are using a depth of 2 – 5 we can calculate the number of voxels involved by each iteration of the step function.

As depicted in algorithm 4 we analyse 3DPFCM.

Lines 1-3: generating a random swarm of particles and running FCM with GMM as cluster centres. This action is a standard FCM evaluation which is $O(\maxIterations \cdot C^2 \cdot N)$

Lines 4-9: we evaluate the objective function which is evaluated by each particle in the swarm SW number of times with d dimensions. The IFCM objective function was $\Theta(C^2 \cdot N)$. In the case of 3DPIFCM the cost is $\Theta(S \cdot C^2 \cdot N)$. The swarm is evaluated \maxIterations or until convergence where the stop criteria is met.

Therefore, the final evaluation of the algorithms is $\Theta(SW \cdot S \cdot d \cdot \maxIterations \cdot C^2 \cdot N)$

Since we define early on that S and d are negligible the evaluation becomes $O(SW \cdot \maxIterations \cdot C^2 \cdot N)$ which is similar to GAIFCM asymptotically.

Nevertheless as stated in [13] and section 4.2.1 the observed runtime performance is faster by a factor of 2.

5 Experiments

5.1 Evaluation parameters

In order to perform a quantitative evaluation of the results three definitions were used in as in the original Shen paper[30]. The evaluation parameters are chosen since we are doing clustering and seek to find if a particular pixel or voxel is in the correct cluster. Table 3 shows the segmentation evaluation parameters.

Table 3: Evaluation parameters

Name of measurement	Formula	Description	Comments
Under Segmentation	$UnS = \frac{N_{fp}}{N_n}$	The percentage of positive false segmentation for a cluster.	N_{fp} – The number of pixels that do not belong to a cluster and are segmented into that cluster (false positives). N_n – The total number of pixels that do not belong to that cluster.
Over Segmentation	$OS = \frac{N_{fn}}{N_p}$	The percentage of negative false segmentation for a cluster.	N_{fn} – The number of pixels that belong to a cluster and are not segmented into that cluster (false negatives). N_p – The total number of pixels that belong to that cluster.
Incorrect Segmentation	$IncS = \frac{UnS + OS}{N}$	The total percentage of false segmentation.	

All our comparisons and evaluations of algorithms are done by the IncS measure. This measure combines both Under Segmentation and Over Segmentation. It is averaged by the total number of pixels/voxels being segmented.

5.2 3DPIFCM accuracy experiments

The experiments section shows a comparison of all algorithms for different noise types and different data types. The purpose of this section is to evaluate the new algorithms in comparison to known implementations. Following evaluations were performed:

- a. We will first define the evaluation parameters for the segmentation quantitatively as defined in the original Shen paper [30].
- b. We will run our 3DPIFCM algorithm against synthetic data as shown in figure 7. We will evaluate using only homogeneous Gaussian noise for this part. The reason for this is that the synthetic data is Uniform and not resembling real data. We perform different noise types such as Gaussian and Poisson in the Brainweb data instead which simulates MRI scans although Poisson noise is more relevant for CT scans.
- c. We evaluate the algorithm on Brainweb data using both Gaussian and Poisson noise types in different levels.
- d. We perform comparative analysis of 3DPIFCM qualitatively against GAIFCM, IFCMPSO, FCM using only incorrect segmentation measure (incS) since it provides a good measure of overall model accuracy.
- e. We summarize the experiments made on h, v hyper parameters.
- f. We analyze the experiments on H parameter which is the exponential decay of voxel's contribution to final clustering and discuss results.
- g. We analyze the experiments on V parameter which is the depth of search between target voxel and search voxel and discuss results.
- h. We present a showcase with visual results comparing 3DPIFCM to the best performing 2D version GAIFCM. We show the segmentation of Brainweb data and compare example executions on different noise levels.
- i. We perform a runtime comparative analysis of all algorithms discussed in this paper.

5.3 Running 3DPIFCM on synthetic data

5.3.1 Purpose

The main goal of running the new algorithm on synthetic data was to test the ability of the algorithm to generalize to different types of data. We ran multiple tests on synthetic volumes presented in section 3.6.

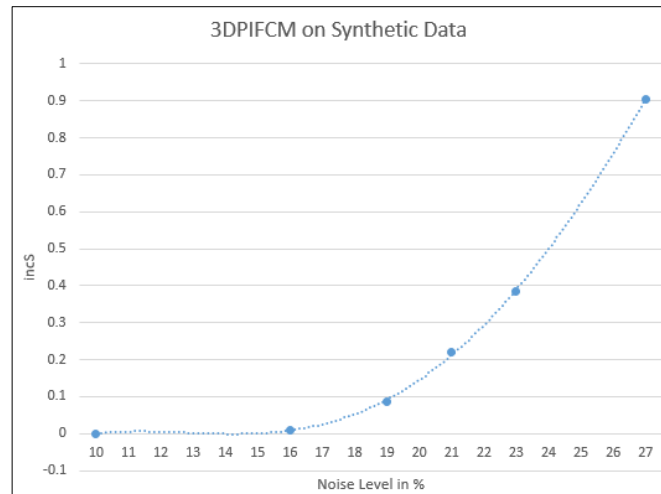
5.3.2 The experiment

We executed the algorithm in different noise levels with varied amounts from 1% to 27% noise. In this experiment only Gaussian noise type was used. An experiment containing an additional noise type was conducted on the synthetic brain data to simulate real world conditions.

5.3.3 Results

We witnessed that below 16% there was no use to show results since the algorithm performed perfect segmentation. Moreover, when testing other FCM variants including FCM we saw the same results below 16% noise. As can be shown in figure 7 on synthetic data under 16% noise there were almost no segmentation errors. The data in the synthetic volume is highly homogeneous and uniform between voxels in the same cluster. Since each cube sits within another outer cube it's easier for the algorithm to use neighborhood attraction of the voxels to determine the right segment. Despite the good results shown in the synthetic volume we expected much more realistic results when looking into Brainweb data which simulates real world brain.

Figure 7: 3DPiFCM on synthetic volume, Includes 10-27% Gaussian noise



5.3.4 Analysis

We can see from the results in figure 7 that in highly correlated images the algorithm which specialized in noisy images performs well. When 16% noise is reached we can see that errors start to occur in segmentation accuracy. This is highly indicative of the stability of the algorithm in different conditions. Although using synthetic generated data is not indicative of real world conditions in medical imaging it gives a good indication of the generality of the algorithm to changing textures and image types. Also, by using highly Uniform data we provide a simple test case to tackle before moving on to simulated brain.

The analysis shows that 3DPiFCM behaves very well on synthetic data and compares well to the original FCM and IFCM variants. There is a steady increase in error rates as noise levels grow beyond 16% showing stable behavior.

5.4 Running 3DPiFCM on Brainweb data

5.4.1 Purpose

The experiment was done with simulated brain volume that gives us ground truth. Since clustering was performed we still require the labels of the pixels/voxels to give us the accuracy of the algorithm. Different noise levels presented by Brainweb ranging from 1% to 20% were used.

The purpose in using both Gaussian and Poisson noise types for those experiments was to accommodate real world conditions which include different image modalities such as CT and MRI. It is known fact that CT scans mainly exhibit Poisson noise[6] while MRI can have Gaussian. In addition, we wanted to measure the effect of different noise types and noise levels on the algorithms' performance in order to assess its ability to generalize to other parts of body and other type of modalities.

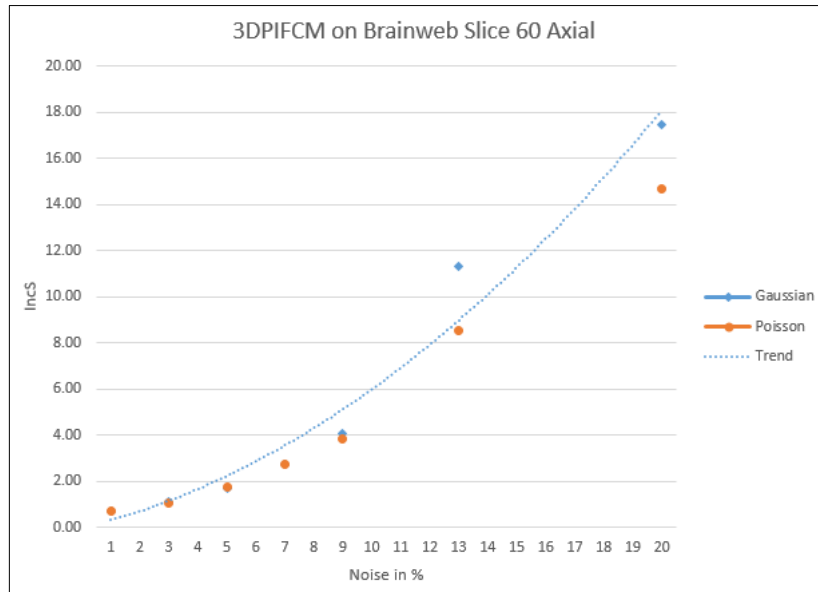
5.4.2 The experiment

We executed the algorithm on Brainweb T1 slice 60 Axial view. We chose this slice as a good middle slice in axial view when the dimension of the entire Brainweb volume was 181x217x181. We used hops of 2% in noise increase from 1% to 9% and additional two executions for 13% and 20% noise. This is so that large noise levels will be examined. Nevertheless, larger noise levels of 13% and 20% are very uncommon as shown in original Shen paper[30].

5.4.3 Results

Results in figure 8 indicate that there is almost a linear relationship between noise levels and error rates when testing against Brainweb data. The two noise types are almost identical for executions of up to 9% where we see a small increase in error rate from 9% onwards for Gaussian noise.

Figure 8: 3DPiFCM on Brainweb T1 volume Slice 60, 1-20% noise (Gaussian and Poisson noise).



5.4.4 Analysis

We can see that the algorithm behaves well in lower noise levels and increases error rates linearly as noise increases. As shown in figure 8, between 13% and 20% noise levels it's very difficult to distinguish between the real voxel information and noise artefacts. Since we focus on real equipment noise (1%-9%) this is acceptable and our goal is to compare this performance to other FCM variants in 2D including FCM itself. As noise level increase from 9% onwards there is clearly better segmentation results for Poisson noise by an increasing margin.

The results indicate that both Poisson and Gaussian noise types are similar in segmentation performance as shown on Brainweb data. Above 9% noise there is a slight advantage to Poisson but since the signal to noise ratio is very low in those levels it is non consequential. Also, a regression line can be seen to fit to the incS as noise levels increase. This indicates that there is a linear relationship between segmentation performance and noise levels.

5.5 Comparative analysis of running 3DPiFCM against FCM, IFCMPSO, GAIFCM

5.5.1 Purpose

We evaluate 3DPiFCM on Brainweb data as shown in section c. We compare the performance of the algorithm using IncS to 3 different algorithms running on 2D images of the same slice. Our algorithm is the only one that is utilizing 3D information as well as the 2D slice. Our main purpose is to compare qualitatively the accuracy of segmentation

with varied amounts of Gaussian and Poisson noise levels. We perform the comparison between each algorithm to 3DPIFCM with formula 13.

$$IncS^{A-3DPIFCM} = \frac{IncS^A - IncS^{3DPIFCM}}{IncS^A} \cdot 100 \quad (13)$$

In formula (13) A is denoted as the the algorithm for comparison. This formula indicates the relative percentage improvement or decrease of 3DPIFCM performance compared to algorithm A. This comparison is done against FCM, IFCMPSO and GAIFCM.

5.5.2 The experiment

As before we evaluate on Gaussian and Poisson noise for all algorithms. We use 1,3,5,7,9,13,20 percent noise levels for all algorithms and compare by IncS error. Figures 11 and 12 show our results on executions of Gaussian and Poisson noise levels respectively. In figure 11 we show a similar experiment that was done on the synthetic data shown in 4.6.

5.5.3 Results

Results show that when comparing to FCM both in Gaussian and Poisson noise we see a dramatic improvement in lower noise levels of 1% up to 9%. The improvement according to (13) is up to 65% peaking in 9% noise and diminishing in 13% noise and higher. When comparing to GAIFCM and IFCMPSO the improvement ranges between 5-20%. Figure 9 shows the comparison on Gaussian noise and figure 10 on Poisson. The negative numbers in figures 9,10 indicates competing algorithms outperform 3DPIFCM by a percentage shown. In figure 11 we show the same experiment and comparison on simulated data shown in section 4.6. We can see an average difference in 31% and 22% against GAIFCM and IFCMPSO respectively across noise levels. Also, as noise grows from 16% to 27% in synthetic data we see a continuous decline in improvement suggesting that noise to signal ration is rapidly diminishing for those noise levels.

Figure 9: Comparison of 3DPIFCM vs FCM, IFCMPSO and GAIFCM at 1-20% Gaussian noise using (13). Using Brainweb T1 Volume slice 60. At noise level 20% GAIFCM outperforms 3DPIFCM by 11%.

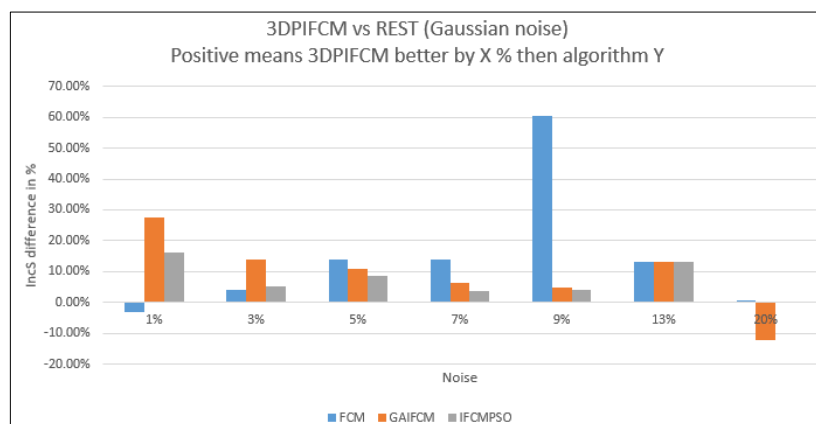


Figure 10: Comparison of 3DPiFCM vs FCM, IFCMPSO and GAIFCM at 1-20% Poisson noise using (13). Using Brainweb T1 Volume slice 60.

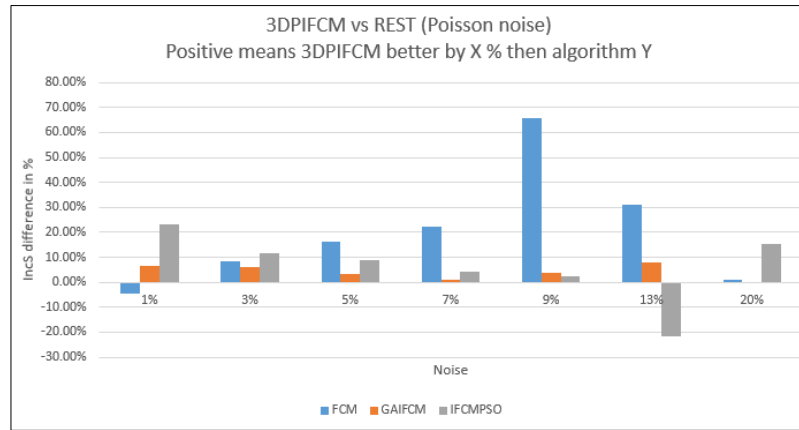
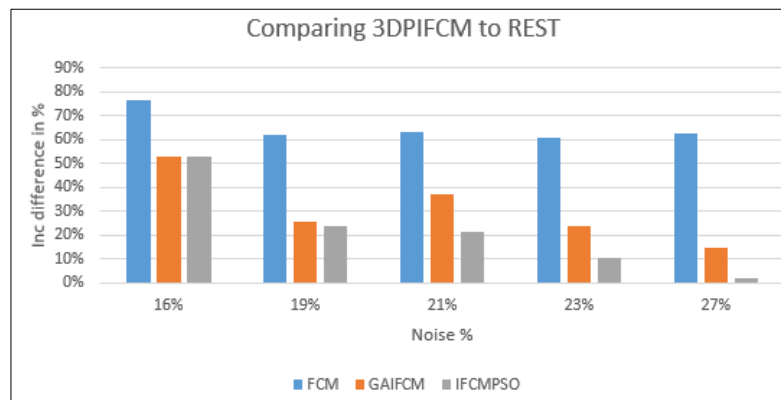


Figure 11: Comparison of 3DPiFCM vs FCM, IFCMPSO and GAIFCM at 16-27%, synthetic data with Gaussian noise using (13).



5.5.4 Analysis

When we analyze the performance of 3DPiFCM against GAIFCM we see an interesting trend. In lower noise levels of 1-13% there is an average improvement of 12% to 3DPiFCM for Gaussian noise. In Poisson noise the situation is a little less dramatic and we see an average of 5% improvement for same levels. In 20% noise levels there is an advantage to GAIFCM of 15% and 12% for Gaussian and Poisson respectively.

Nevertheless, even FCM only performs at a similar level to 3DPiFCM at 20% noise. This suggests that the 3D nature of the algorithm which collects voxels in 3 dimensions per iteration abstracts its performance at very high noise levels. Also, as can be seen in both [30] and in our paper section 4.6, in 20% the image is almost indistinguishable from noise.

In synthetic data the results show similar characteristics. We perform the comparison on 16%-27% and see a decline in improvement as noise levels grow to 27% and beyond.

5.6 Evaluating new Dynamic Hyper parameters

5.6.1 Purpose

As described in table 2 there are two new hyper parameters in 3DPIFCM. The effect of those parameters on the overall accuracy of the algorithm was researched. Each parameter was analyzed separately. To do this we modified other parameters during the executions and took the average or minimum execution for each parameter value depending on the experiment performed.

5.6.2 Hyper parameter H

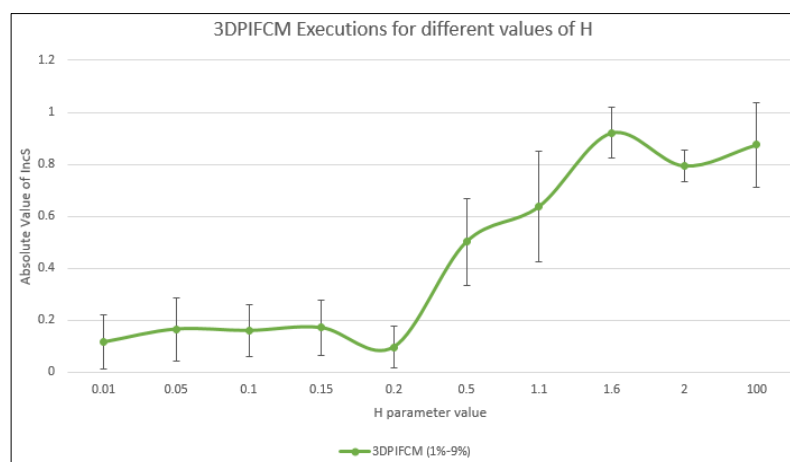
5.6.2.1 The experiment

The 3DPIFCM algorithm was run on Simulated brain data T1 Axial view on slice 60. We selected this slice as it is a central slice of the brain and representative for segmentation. Additional analysis is illustrated in figure 18 on slice number 100. The H parameter was changed, and all other values remained the same for the sake of the experiment. Values ranging from 0.01 to 100 were chosen through multiple iterations. After testing the effect we can see that a low value such as 0.01 will give a very high weight to the first order of voxels and a much lower weight to next levels. The effect will be that closer voxels will affect the segmentation of the target voxel much more than far ones. In the same manner if we use an H value of 100 than the weigh is distributed evenly between far voxels and close voxels thus having similar effect on the segmentation.

In our experiments for each value of H we executed a series of runs of the algorithm with different noise levels ranging from 1%-20%. In figure 12 we can see the execution of the algorithm on noise levels 1%-9%. We omit the 13%-20% because we there was a very high standard deviation on the results of each execution in different H levels and because as mentioned in previous sections at those noise levels the algorithm reduces accuracy to near FCM level.

5.6.2.2 Results

Figure 12: Execution of 3DPIFCM with different values of H ranging between 0.01 and 100. The experiment ran on Brainweb T1 Volume in slice 60 Axial view with Gaussian noise. We average executions for noise levels 1%-9%.



5.6.2.3 Analysis

There is a saddle point when a value of 0.2 is reached. This suggests that there is a local optimum for this value in Brainweb data for different noise levels. Also, above 0.2 there is a steady increase in error rates regardless of the amount of noise suggesting that if we distribute the weights between far and near voxels more evenly it will reach a point that clustering performance will be degraded.

Since there is a local optimum for h parameter in this data type, it can be assumed that for similar data types of other modalities we could also find local optimums. As a result, different values of h can be preconfigured for different modalities and body types in images.

5.7 3D depth- V parameter

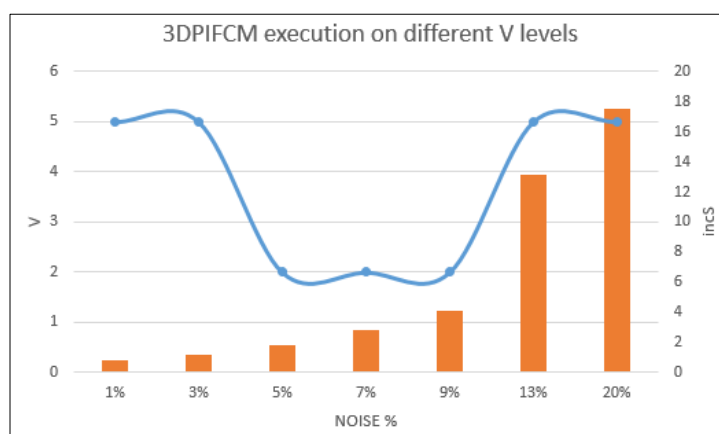
5.7.1 The experiment

In this experiment the noise level increased between 1%-20% and the best performing V value was taken for each noise level which minimized incS. If the H parameter described the weight of X order voxels from target voxel, V represents the depth of the search per voxel in each iteration of the algorithm. In this experiment values of V ranged between 2 and 5. The lower value was chosen similar to [30][10][5] while the higher value was the highest possible value given the memory constraints of the server. All other parameters in the experiment remained the same. In our earlier tests we saw that a larger number than 5 will significantly increase computation time and not improve performance.

If we calculate the number of voxels that need to be examined per iteration for the v value the numbers are as follows, for v=2 there are 18 voxels in the search space, v=3 there are 26 voxels, v=4 there are 92 voxels and finally for v=5 there are 116 voxels. This is partly shown in figure 4. This series is an exponential series and computation time is affected significantly if we go beyond 5. Figure 13 shows the effect of the V parameter for different noise levels ranging from 1% to 20%. All experiments ran on Brainweb T1 Volume slice 60.

5.7.2 Results

Figure 13: Execution of 3DPFCM on Brainweb T1 slice 60 Gaussian noise for different noise levels taking the minimum for each V value.



5.7.3 Analysis

From figure 15 we can see that for lower noise levels the best performance is gained by using a higher v . For middle noise between %5-%9 a low value is more performant. In high noise levels of %13-%20 we can witness an additional rise in this parameter. This suggests that high noise levels are not sensitive to the depth parameter since the noisy voxels block the information from reaching the central voxel being evaluated. As a result we could formulate the pre selection of this value depending on known noise level as default.

The results of this experiment indicate that there is an optimal value for the v parameter per noise level and per modality type. It can be concluded that a preselection step can be performed according to noise and image types and default values can be chosen before executing 3DPiFCM on a new data set.

5.8 Parallel 3DPiFCM experiments

5.8.1 Introduction

The goal of this experiment was to test for parallel 3DPiFCM against various algorithms that were shown in this work. The comparison metric is execution speed in seconds given that all other parameters are the same for each algorithm. In order to ensure that the GPU version is comparative to the CPU version in quality few tests were conducted on various images and got similar segmentation results between the two. All CPU versions were optimized via numba framework in the same way as the GPU version. Threading was not used both in CPU and GPU versions.

The algorithms we compared against are shown in table 4. Each test was conducted several times and average speed was taken. Since the FCM version is doing no parameter optimization and noise reduction it was significantly faster than the rest of the algorithms including the GPU version. However, in the experiments we show that the GPU version can run in reasonable time whereas the other CPU generic variants significantly degrade in runtime as the images increase in size.

Table 4: algorithms comparison

Algorithm Name	Description	Features	Hardware
FCM[5]	Standard Fuzzy C Means Clustering (implementation in Python)	2D features of intensity difference between pixels only. This is original FCM which has no optimization parameters.	CPU only
IFCMPSO[9]	IFCM with Particle Swarm Optimization of parameters λ and ξ . We use same parameters for PSO for IFCM-PSO, 3DPIFCM, 3DPIFCM-GPU.	2D features, PSO optimization of λ and ξ . This is original IFCM with PSO optimization which doesn't use V, h, g parameters.	CPU only
3DPIFCM	IFCM with Particle Swarm Optimization with 3D features and optimization parameters. This is our incarnation of the algorithm with 3D features for noise reduction.	3D features, PSO optimization of λ, ξ . In addition, testing different configurations of V, h, g parameters for performance tuning.	CPU only
3DPIFCM-GPU	This is a new implementation of 3DPIFCM on a GPU. We use several techniques and move the image entirely to the GPU memory and perform parallel computation there.	3D features, PSO optimization of λ, ξ . In addition, testing different configurations of V, h, g parameters for performance tuning.	CPU and GPU combination. Sequential part on CPU and parallel on GPU.

All the implementations of the algorithms were done in python with Numba[18] JIT compilation for the segmentation parts. The runtime is comparable to native C versions since we used heavy optimization of scientific libraries such as Numpy[24] and Numba which are native implementations. The GPU CUDA version was also JIT compiled using Numba directives on kernel functions. All algorithms we compared against including 3DPIFCM – CPU run on an 8 core CPU with 64 GB of memory and a TITAN X GPU with 3072 SP cores and 12GB of memory. The following sections describe the experiments.

5.8.2 Synthetic Volume experiment

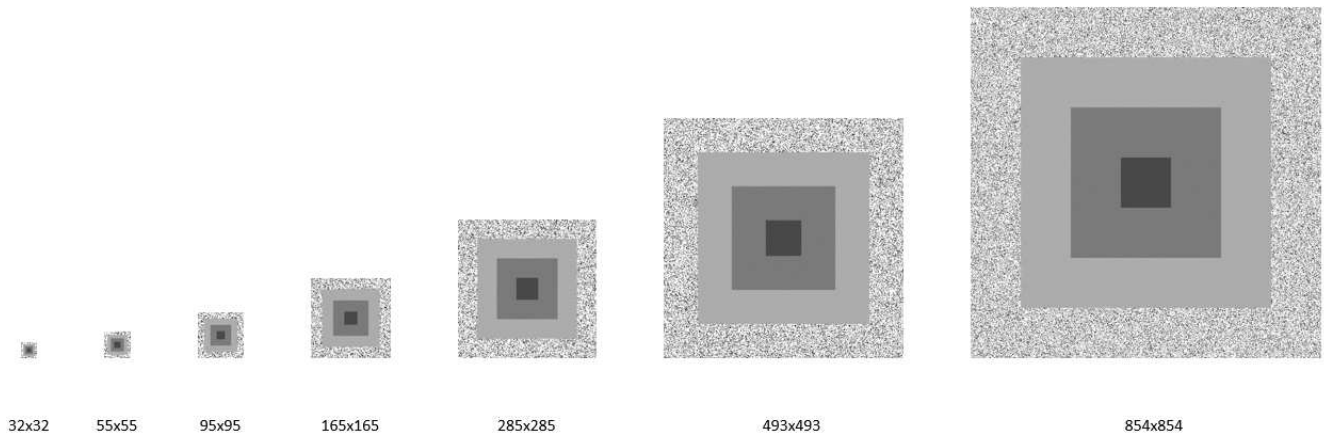
5.8.2.1 Goal

The goal of this experiment was to show the relationship between size of an image and speed of execution between parallel version of 3DPIFCM and other IFCM variants including FCM.

5.8.2.2 Method

A synthetic dataset was used showed in 4.6. The dataset is a cube with in a cube with ranging grayscale colors in 3D space. The size of the images in the original dataset is 181x217x181 voxels. In the experiments GPU speed was tested with ranging image sizes. Thus we recreated the dataset with varied sizes of 32x32, 55x55, 95x95, 165x165, 285x285, 493x493, 854x854. The images double in sizes to examine the speed with which all algorithms can handle the segmentation and optimization. Figure 14 shows the synthetic images.

Figure 14: synthetic images for execution speed comparison between various algorithms.



5.8.2.3 Results

A comparison of those different executions is shown in figure 15 and table 4.

Figure 15: Visual comparison in execution speed between all algorithms.

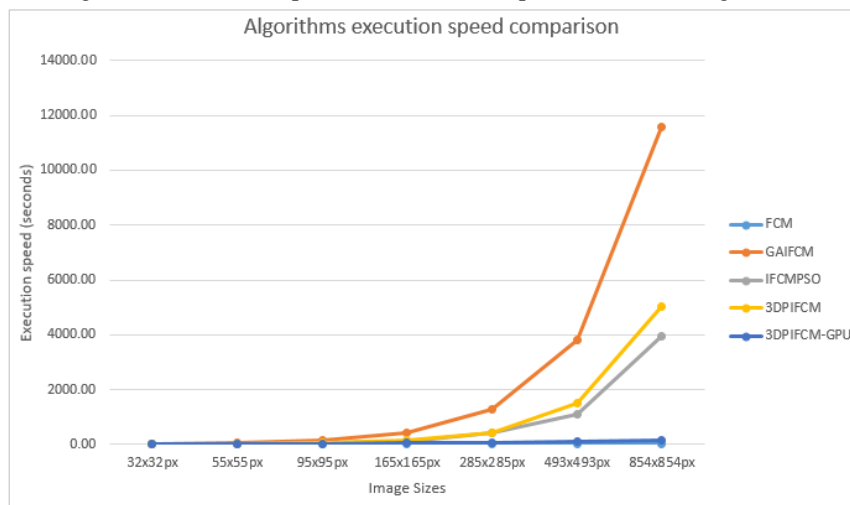


Table 4: Execution time [seconds] comparison on synthetic data

Size	FCM	GAIFCM	IFCMPSO	3DP IFCM	3DP IFCM-GPU
32x32px	0.02	15.95	4.62	6.66	7.44
55x55px	0.05	49.20	11.24	12.75	10.80
95x95px	0.15	146.39	40.53	46.86	17.27
165x165px	0.53	442.48	99.58	142.55	41.57
285x285px	1.79	1290.96	413.09	422.42	48.81
493x493px	9.01	3794.71	1086.06	1501.91	89.47
854x854px	24.56	11570.61	3958.05	5033.24	170.60

5.8.2.4 Analysis of results

As can be seen from figure 15 for small images there is a small overhead of moving the image to the GPU for parallel processing. As the images increase there is a significant benefit in running the GPU version. In fact we can see that for average image sizes of 285x285 there is an increase of 27x in speed compared to GAIFCM, 8.5x increase compared to IFCMPSO and 8.6x increase compared to the CPU version of 3DPIDFCM. When we reach maximal size we see that the speed increase is 68x compared to GAIFCM, 23x for IFCMPSO and 29x for 3DPIDFCM in CPU version. The advantage in these results is that as images in medical modalities become larger in sizes due to modern equipment and accuracy of devices parallel algorithms such as 3DPIDFCM will start gaining more traction and implementation in clinical settings will be more frequent. The results show that 3DPIDFCM is good candidate for clinical settings because of balance between speed and accuracy.

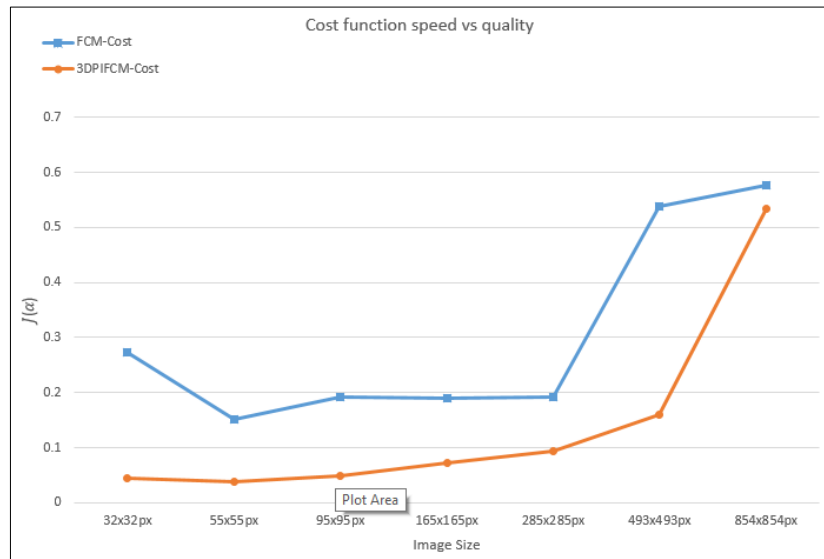
As can be seen in table 4 the FCM algorithm outperforms all IFCM variants including parallel 3DPIDFCM in execution speed. However, as we showed in 5.6.3 it begins to degrade in accuracy as noise is introduced into the image. In order to adequately show a tradeoff between speed and quality in noisy images we create a cost function (14) to establish benefit of 3DPIDFCM across different image sizes. The cost function trades off incorrect segmentation ($incS$) and execution speed in seconds (S). We trade execution speed for quality as there is a significant clinical advantage to speedy results for handling the patient.

$$J(\alpha) = \frac{1}{k} \sum_{i=1}^k \alpha \left(\frac{incS_i - \min(incS)_i}{\max(incS)_i - \min(incS)_i} \right) + (1 - \alpha) \left(\frac{S_i - \min(S)_i}{\max(S)_i - \min(S)_i} \right) \quad (14)$$

We introduce the α variable to account for weight of $incS$ in regards to final cost. If α is close to 1 than most weight is contributed to quality and less for speed. If α is closer to 0 most weight contributed to speed. The variable k is the number of different image sizes, in our experiment $k=7$. Within the parenthesis of each expression we perform min max normalization of speed and $incS$ to scale between 0 and 1. In figure 16 we show the cost function for different image sizes by averaging 3-9% noise levels. In this figure we set the α value to 0.7 to give the more weight to quality and less to speed.

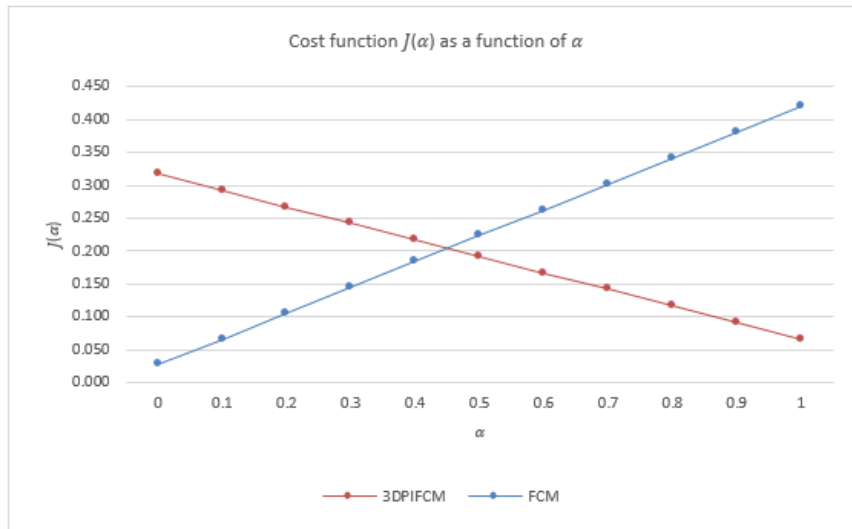
Figure 16: Cost function $J(\alpha)$ for different image sizes with $\alpha = 0.7$.

of Gaussian noises between 3% to 9%.



It can be seen that there is a constant margin in cost between FCM and 3DPICM in all noise levels on average. We also examine the cost function as a function of different values of α in figure 17. We can see that the cost of FCM is increasing above 3DPICM beyond a value of 0.45 and trending up while the cost of 3DPICM is trending down as α increases.

Figure 17: Average Cost function $J(\alpha)$ as a function of α for k different images. Average Gaussian noises between 3% to 9%



5.8.2.5 Conclusion

From experiments above it can be shown that 3DPICM parallel implementation is faster than all other IFCM variants when the image size is above 55x55 pixels. FCM outperforms parallel 3DPICM in speed but fails in quality when using noisy images. A tradeoff function was shown to compare between the two algorithms in terms of quality and speed of execution. We tested different levels of noise ranging between 3% to 9% Gaussian noise and averaged the results across levels. Above 9% noise the image loses information as we showed in 5.6. Below 3% there is no advantage to IFCM or its variants because FCM performs good enough. The tradeoff function shows a clear advantage to 3DPICM for noisy images even when α is small and tends towards speed. This is primarily because the speed benefit of FCM is much less than the quality benefit of 3DPICM given the same conditions in noisy images. We can see a clear trend in (α) with advantage to 3DPICM as the quality component grows.

5.8.3 Brainweb Volume Experiment

5.8.3.1 The Goal

The goal of this experiment was to show realistic conditions by using a simulated MRI brain volume from Brainweb. Real data was not used as it comes unlabeled and it's very expensive to label each pixel in real settings. Because real data such as Brain MRI scan contains many different gray levels and inconsistencies within colors it may present different results from a simulated image.

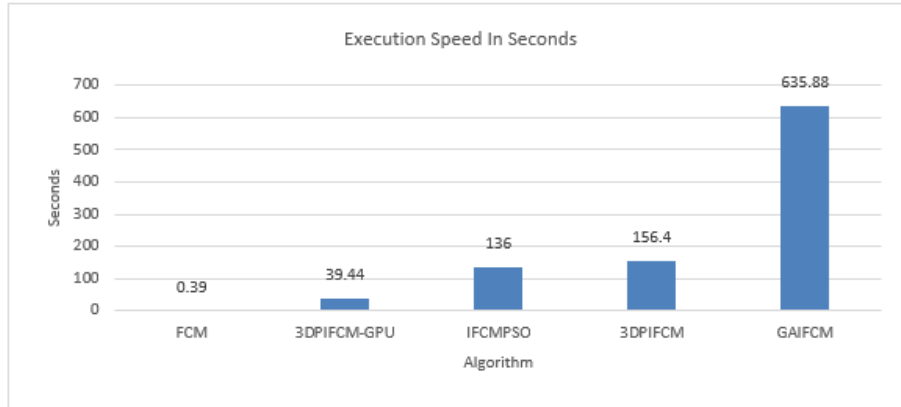
5.8.3.2 Method

Standard Brainweb [7] volume was used in this experiment. It was the same data used in 5.4. The size of the 3D images there are 181x217 on the axial z axis.

5.8.3.3 Results

We can see the execution results from Brainweb in figure 18.

Figure 18: Comparison of algorithms in Brainweb slice 100 with 7% Gaussian noise.



5.8.3.4 Analysis of results

As we can see, the FCM version is performing considerably faster even when executing on a CPU with JIT compilation enabled. However, as we showed in this paper there is a degradation in segmentation quality for FCM when noise levels increase above 1%. The increase in quality of segmentation between FCM and 3DPIFCM on the GPU is 4.6x which is considerable when taking into account the medical implications of incorrect segmentation.

We can clearly see that the GPU version outperforms the CPU version by a factor of 4. When we compare to IFCMPSO on CPU version we get a 3.5x increase in speed and 16x increase compared to GAIFCM for the same volume. Since the speedup is dependent on specific hardware setup and GPU we would like to give a theoretical foundation to the potential benefits of parallel 3DPIFCM. We use a modified Amdahl's Law [3] to test the benefits because our algorithm has both sequential and parallel parts.

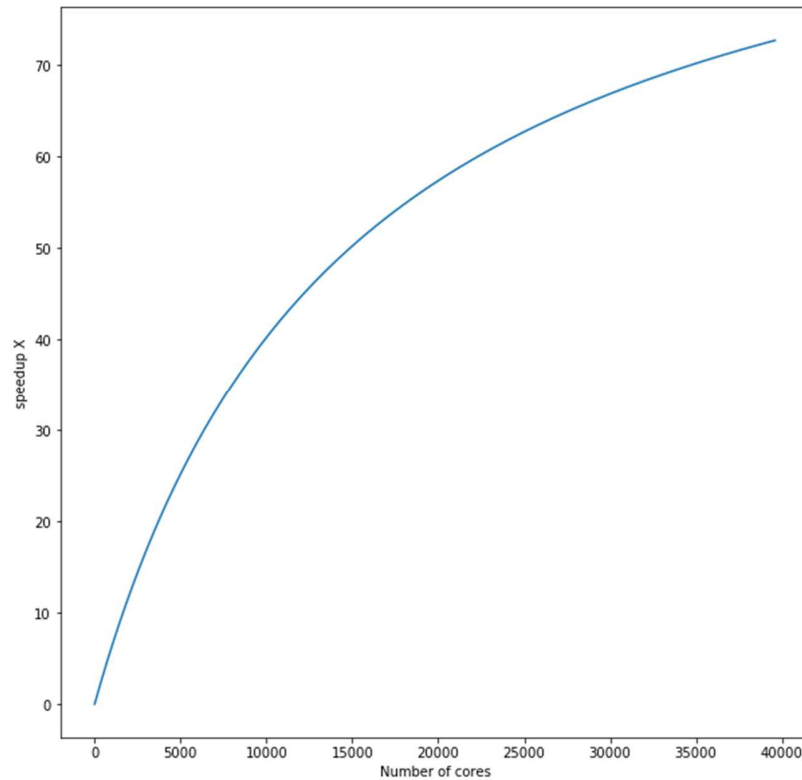
$$S_{latency}(s) = \frac{1}{(1 - p) + \frac{kp}{jN}} \quad (15)$$

This formula gives the potential benefit of a parallel version of an algorithm given the following variables:

- p – The proportion of execution time that the part benefiting from improved resources originally occupied.
- N – Number of processors.
- k – The ratio between CPU clock speed and GPU clock speed per processor.
- j – The ratio of data transfer between CPU to GPU.

In order to show the benefits several assumptions were made regarding the parameters of this formula. First, the ratio k is set to 3. This assumption is made by testing current modern GPU's which have roughly one third the clock speed of a CPU. Second, we set p to 0.99. p is the proportion of execution time that the part we make parallel uses. In case of 3DPIFCM 99% reflects that most time is spent on the kernel part. In addition, we set j which is the ratio between algorithm running time and data transfer to 1/50. In figure 19 we show the potential benefits of speedup as N grows. This means that we increase the number of GPU SP cores.

Figure 19: Speedup of 3DPFCM as a function of number of cores



5.8.3.5 Conclusion

In this experiment it was shown that 3DPFCM can perform well in real world conditions against known IFCM variants while increasing speed. Also, it was shown that the algorithm can be used in clinical settings. In real MRI images the Gaussian noise factor normally ranging between 1-10% [7]. When executing 3DPFCM in parallel mode on the GPU we saw a constant ratio in speed increase regardless of the noise component in the image. This can be shown well both in figure 15 and table 4.

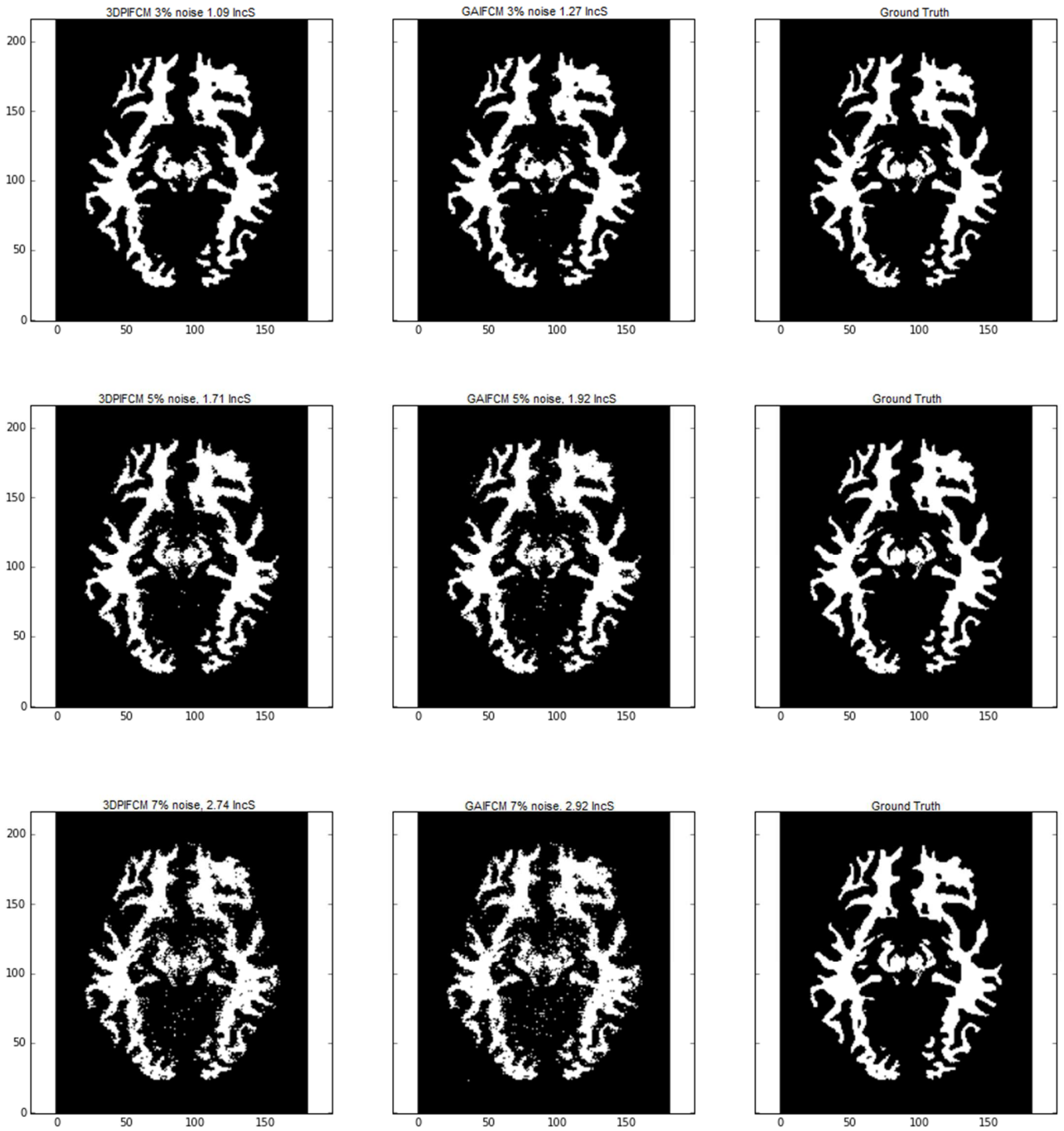
6 Case Study

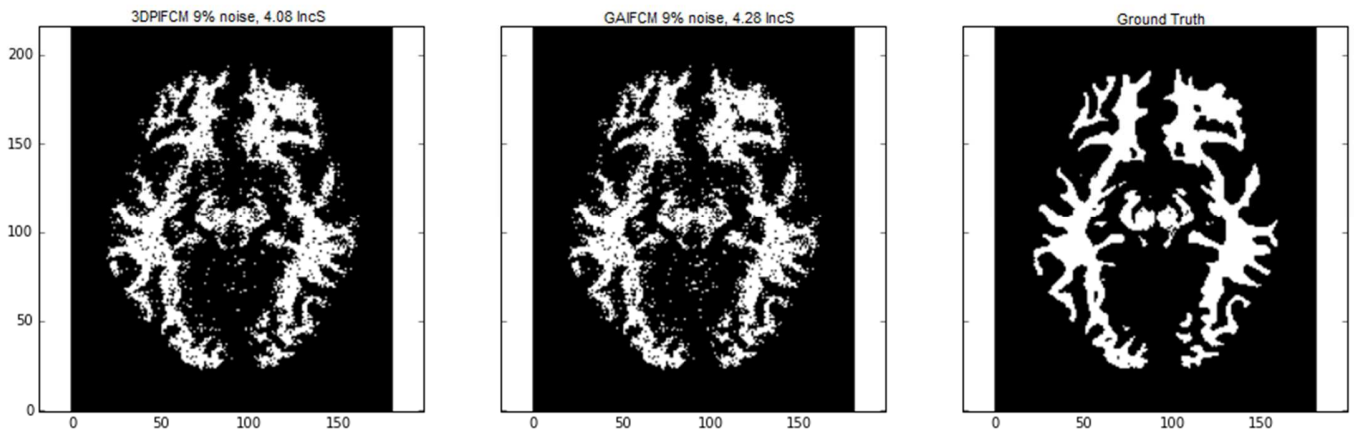
6.1 Purpose

One of our goals was to test 3DPFCM qualitatively against the other algorithms with varied noise levels. To perform such a test we segmented an adult brain slice in Brainweb[7] with all algorithms and took the WM (white matter) segmentation as a test case. The reasoning behind this approach is to view the results more clearly with a naked eye and compare which pixels were misclassified in each algorithm. Figure 20 shows a comparison of 3DPFCM against GAIFCM for WM. Again, for sake of brevity we remove the 1% noise comparison for lower bound and over 9% noise for upper bound. Results in those bounds are very difficult to visualize and provide no added value to our analysis.

6.2 Results

Figure 20: comparison of 3DPIFCM and GAIFCM with different noise levels ranging from 3% to 9% with Gaussian noise.





6.3 Analysis

We can see in the results that edge cases where the clusters are close to each other 3DPiFCM performs better because of the higher noise reduction capability as a result of 3D corrections. From 13% noise and higher the quality of image degrades to a level that it's almost indistinguishable between noise artifacts and real pixels.

For this reason in figure 20 we show only noise levels of 3%-9%. We omitted 1% noise since results were almost indistinguishable and not visible enough. Also, above 9% there is no clear advantage to 3DPiFCM mostly because of low noise to signal ratio.

In conclusion, all comparisons in the case study show that the mean of error difference between 3DPiFCM and GAiFCM is 0.19 in incS with standard deviation of 0.012. This means that there is a constant gap of 0.2% absolute error rate reduction in advantage to 3DPiFCM compared to GA. In addition, it can be seen that the error is evenly distributed in the images. This indicates that the performance increase is not due to local advantage but as a result of either the optimization algorithm or the additional 3D features that make the algorithm more noise resistant.

7 Limitations

The limitations of our study were:

1. Usage of only simulated brain data for real world example but not actual brain MRI. This was because it was critical to measure accuracy in comparison to other algorithms based on accurate labeling, which came with simulated Brainweb data.
2. Using a specific hardware and software setting to compare speed. It can be difficult to generalize exact speedups in different environments with different constraints.
3. Comparison was made with similar clustering algorithms using different optimization techniques to account for noise. We didn't test accuracy against a completely different segmentation paradigm like region growing or supervised deep learning.
4. Using python with scientific package and JIT compilation might not be the most optimal language to test for speed when comparing similar algorithms. The best choice might be to implement all algorithms in a native language such as C or C++.
5. We used a limited parallel environment by using a single GPU. Theoretically many GPUs can be used if distributing the computation correctly. This could lead to additional potential speedups.
6. Additional algorithms can be tested using parallel settings by using this initial work.

Overall our study represents a general approach to clustering given noisy artifacts in medical images. The limitations presented above could all be mitigated by data enhancement, change of hardware and software, and lastly additional computational resources with many GPUs as setup.

8 Conclusions

In this paper we introduced a new segmentation algorithm that is based on IFCM and particle swarm optimization. The purpose of this algorithm was to gain accurate segmentation in 3D images that contain noise due to intensity inhomogeneity or a bias field such as MRI and CT scans. The algorithm is unsupervised and requires no training data. As a result, it can be a good fit for clustering images where there is a small number of labeled examples available. The algorithm uses 3D features in order to counter the noisy slices produced by the equipment. To evaluate the performance of this algorithm we tested on both synthetic and Brainweb data.

We showed that the algorithm outperforms state of the art genetic variants such as GAIFCM and IFCMPSO by a margin of 5-50% improvement for synthetic data and 1-28% improvement for simulated brain data using the standard incorrect segmentation which is the percentage of false segmented pixels in the image. We compare Gaussian and Poisson noise functions separately on all the datasets to gain higher confidence on segmentation ability and noise reduction. We showed that our algorithm utilizes the 3D nature of the image hence gaining more information about the surrounding voxels during each iteration and as a result performs with higher quality. Also, we showed that the algorithm works best for medium noise levels 3-10% which are most common as shown in Brainweb. The results show that in very low noise of 0-1% there is no advantage over FCM or other genetic variants because the attraction features are not performing noise reduction and in fact reduce accuracy.

In addition, we observed that in very high noise levels of 20% and above there is no significant difference between standard FCM and the noise reduction variants. We suspect that this is because of very low signal to noise ratio which prevents noise reduction to be effective. In addition to introducing 3DPICM we also evaluate two new hyper parameters which control the depth of search from target voxel and the exponential decay of a contribution of each voxel to the overall clustering. We evaluated those parameters in different noise levels and show that there can be optimum values depending on noise levels and image type. This suggests that the algorithm can be preconfigured with default values in the future according to image types and noise types.

We also present a case study of qualitative results of WM comparison between GAIFCM and 3DPICM. We see that in areas in between clusters GAIFCM can misclassify. This suggests that our 3D version which can look at top and bottom slices in the z index can account for the noise artifacts better than 2D variants and therefore is more accurate around the edges and in between the clusters.

In addition to the sequential version of 3DPICM we introduced a parallel version using GPU CUDA computation environment. We showed that in specific GPU and CPU setting the GPU version is comparative in quality to the CPU. Nevertheless, it's up to 68x faster than the slowest IFCM variant. For average sized images of 285x285 it's 15x faster than other IFCM variants on average including the same algorithm's implementation on a CPU. When we compared the algorithms on a Brainweb T1 volume of size 181x217, axial view, we reached an increase in 4.6x in quality compared to FCM and speedup of up to 16x compared to GAIFCM and 3.5x compared to IFCMPSO.

In addition, we gave theoretical foundation using Amdahl's Law with certain assumptions suggesting a much bigger speedup given more SP cores and faster GPU. In this setting it is possible to reach 100x speedup by using 15000 SP cores in the future instead of 3500 as of writing this paper.

The parallel 3DPICM performs well in clinical settings and achieves state of the art quality segmentation in noisy images. We introduced a new cost function to compare between two algorithms by factoring noise and segmentation quality. The 3DPICM algorithm has a clear advantage over FCM when we compare against speed and quality in noisy images. This algorithm opens a new door for clinical parallel algorithms for image segmentation that utilize modern computational environments.

9 Further Research

In this research we evaluated 3DPIFCM against other genetic segmentation algorithms such as GAIFCM and IFCMPSO that reduce noise from 2D images. We used Simulated Brain MRI images which normally come in 3D image formats such as Nifti or MINC. We would like to evaluate the algorithm on different sets of organs with ground truth both in CT scans and MRI scans to gain better understanding of the generalization ability of the algorithm in different conditions. Additional qualitative evaluation would be to check segmentation results by doctors and qualified medical staff to further establish credibility and assess the quality of the algorithm.

Some further steps for our research include a fully native implementation of 3DPIFCM on either C or C++ which may increase execution performance further. In addition, we would like to utilize shared memory as shown in [2] for better utilization of the GPU internals. The shared memory as shown in [2] is 100 times faster than global device memory and can significantly increase the step function's performance further. Also, we would like to test on different images modalities such as CT and Ultrasound of different sizes. This would validate our approach for noisy images segmentation and promote a clinical settings experiment.

10 References

- [1] Al-Ayyoub, Mahmoud, et al. "A gpu-based implementations of the fuzzy c-means algorithms for medical image segmentation." *The Journal of Supercomputing* 71.8 (2015): 3149-3162.
- [2] Almazrooie, Mishal, Mogana Vadiveloo, and Rosni Abdullah. "GPU-Based Fuzzy C-Means Clustering Algorithm for Image Segmentation." *arXiv preprint arXiv:1601.00072* (2016).
- [3] Amdahl, Gene M. "Validity of the single processor approach to achieving large scale computing capabilities." *Proceedings of the April 18-20, 1967, spring joint computer conference*. ACM, 1967.
- [4] Benaichouche, Ahmed Nasreddine, Hamouche Oulhadj, and Patrick Siarry. "Improved spatial fuzzy c-means clustering for image segmentation using PSO initialization, Mahalanobis distance and post-segmentation correction." *Digital Signal Processing* 23.5 (2013): 1390-1400.
- [5] Bezdek, James C., Robert Ehrlich, and William Full. "FCM: The fuzzy c-means clustering algorithm." *Computers & Geosciences* 10.2-3 (1984): 191-203.
- [6] Boas, F. Edward, and Dominik Fleischmann. "CT artifacts: causes and reduction techniques." *Imaging Med* 4.2 (2012): 229-240.
- [7] Cocosco, Chris A., et al. "Brainweb: Online interface to a 3D MRI simulated brain database." *NeuroImage*. 1997.
- [8] de Moraes, Thiago F., et al. "InVesalius: An open-source imaging application." *Computational Vision and Medical Image Processing: VipIMAGE 2011* (2011): 405.
- [9] Forouzanfar, Mohamad, Nosratallah Forghani, and Mohammad Teshnehlab. "Parameter optimization of improved fuzzy c-means clustering algorithm for brain MR image segmentation." *Engineering Applications of Artificial Intelligence* 23.2 (2010): 160-168.
- [10] Frizon S, Herman M, Last M. "GAIFCM Algorithm for MRI Fetal Brain Image Segmentation" Master thesis, Open University, Israel (2015).
- [11] Garland, Michael, et al. "Parallel computing experiences with CUDA." *IEEE micro* 28.4 (2008).
- [12] Gupta, Lalit, and Thotsapon Sortrakul. "A Gaussian-mixture-based image segmentation algorithm." *Pattern Recognition* 31.3 (1998): 315-325.
- [13] Hassan, Rania, et al. "A comparison of particle swarm optimization and the genetic algorithm." *Proceedings of the 1st AIAA multidisciplinary design optimization specialist conference*. 2005.
- [14] Jamshidi , Pilevar, Automatic Segmentation of Medical Images Using Fuzzy c-Means and the Genetic Algorithm, *Journal of Computational Medicine*, Article ID 972970, Vol. 2013
- [15] Kaur, Amanpreet, and M. D. Singh. "An overview of pso-based approaches in image segmentation." *Int J Eng Technol* 2.8 (2012): 1349-1357.
- [16] Keh-Shih Chuang, Hong-Long Tzeng, Sharon Chen, Jay Wu, Tzong-Jer Chen "Fuzzy c-means clustering with spatial information for image segmentation" *Computerized Medical Imaging and Graphics* Vol. 30, 9–15, 2006
- [17] Kennedy, James. "Particle swarm optimization." *Encyclopedia of machine learning*. Springer US, 2011. 760-766.
- [18] Lam, Siu Kwan, Antoine Pitrou, and Stanley Seibert. "Numba: A llvm-based python jit compiler." *Proceedings of the Second Workshop on the LLVM Compiler Infrastructure in HPC*. ACM, 2015.

- [19] Leike, Arnd. "Demonstration of the exponential decay law using beer froth." *European Journal of Physics* 23.1 (2001): 21.
- [20] Li, Haiyang, Zhaofeng Yang, and Hongzhou He. "An Improved Image Segmentation Algorithm Based on GPU Parallel Computing." *JSW* 9.8 (2014): 1985-1990.
- [21] Liu, Jiansheng, and Shangping Qiao. "A image segmentation algorithm based on differential evolution particle swarm optimization fuzzy c-means clustering." *Computer Science and Information Systems* 12.2 (2015): 873-893.
- [22] Neelin, P. "The MINC file format: from bytes to brains." *NeuroImage* 7 (1998): P-0786.
- [23] Niu, Qiang, and Xinjian Huang. "An improved fuzzy C-means clustering algorithm based on PSO." *Journal of Software* 6.5 (2011): 873-879.
- [24] NumPy, Developers. "NumPy." NumPy Numpy. Scipy Developers (2013).
- [25] Nvidia, C. U. D. A. "Compute unified device architecture programming guide." (2007).
- [26] Oliphant, Travis. "Numba python bytecode to LLVM translator." *Proceedings of the Python for Scientific Computing Conference (SciPy)*. 2012.
- [27] Patil, Dinesh D., and Sonal G. Deore. "Medical image segmentation: a review." *International Journal of Computer Science and Mobile Computing* 2.1 (2013): 22-27.
- [28] Rowi ska Z, Gocawski J Cuda based fuzzy c-means acceleration for the segmentation of n images with fungus grown in foam matrices. *Image Processing and Communications* 17(4):191200. DOI:10.2478/V10248-012-0046-7, 2012.
- [29] Shalom, S.A.A., Dash, M. and Tue, M. Graphics hardware based efficient and scalable fuzzy c-means clustering. <http://dx.doi.org/10.1007/s11227-015-1431-y>. In *Proceedings of the 7th Australasian data mining conference*, volume 87, Australian Computer Society Inc, Darlinghurst, Australia, AusDM 08, pp 179186. 2008.
- [30] Shen, Shan, et al. "MRI fuzzy segmentation of brain tissue using neighborhood attraction with neural-network optimization." *Information Technology in Biomedicine, IEEE Transactions on* 9.3 (2005): 459-467.
- [31] Smistad, Erik, et al. "Medical image segmentation on GPUs—A comprehensive review." *Medical image analysis* 20.1 (2015): 1-18.
- [32] Soroosh 129/GPU-FCM, <https://github.com/Soroosh129/GPU-FCM>. Retrieved 10 May 2015.
- [33] Wilt, Nicholas. *The cuda handbook: A comprehensive guide to gpu programming*. Pearson Education, 2013.
- [34] Zhang, Jian, and Ling Shen. "An improved fuzzy c-means clustering algorithm based on shadowed sets and PSO." *Computational intelligence and neuroscience* 2014 (2014): 22.405.
- [35] Bali, Akanksha, and Shailendra Narayan Singh. "A review on the strategies and techniques of image segmentation." *2015 Fifth International Conference on Advanced Computing & Communication Technologies*. IEEE, 2015.